Interpreting Observed Temperature Probability Distributions Using a Relationship between Temperature and Temperature Advection

BOER ZHANG,[a] MARIANNA LINZ,[a,b] and GANG CHEN[c]

[a] *School of Engineering and Applied Sciences, Harvard University, Cambridge, Massachusetts*
[b] *Department of Earth and Planetary Sciences, Harvard University, Cambridge, Massachusetts*
[c] *Department of Atmospheric and Oceanic Sciences, University of California, Los Angeles, Los Angeles, California*

(Manuscript received 30 November 2020, in final form 19 October 2021)

ABSTRACT: The nonnormality of temperature probability distributions and the physics that drive it are important due to their relationships to the frequency of extreme warm and cold events. Here we use a conditional mean framework to explore how horizontal temperature advection and other physical processes work together to control the shape of daily temperature distributions during 1979–2019 in the ERA5 dataset for both JJA and DJF. We demonstrate that the temperature distribution in the middle and high latitudes can largely be linearly explained by the conditional mean horizontal temperature advection with the simple treatment of other processes as a Newtonian relaxation with a spatially variant relaxation time scale and equilibrium temperature. We analyze the role of different transient and stationary components of the horizontal temperature advection in affecting the shape of temperature distributions. The anomalous advection of the stationary temperature gradient has a dominant effect in influencing temperature variance, while both that term and the covariance between anomalous wind and anomalous temperature have significant effects on temperature skewness. While this simple method works well over most of the ocean, the advection–temperature relationship is more complicated over land. We classify land regions with different advection–temperature relationships under our framework, and find that for both seasons the aforementioned linear relationship can explain ~30% of land area, and can explain either the lower or the upper half of temperature distributions in an additional ~30% of land area. Identifying the regions where temperature advection explains shapes of temperature distributions well will help us gain more confidence in understanding the future change of temperature distributions and extreme events.

KEYWORDS: Advection; Atmospheric circulation; Dynamics; Climate change; Climate classification/regimes; Temperature

1. Introduction

Although climate change is described in terms of global mean warming (e.g., 2°C), its impacts depend on the local changes to both the mean temperature and the temperature distribution. Recent observations (McKinnon et al. 2016; Rhines et al. 2017) and simulations (Tamarin-Brodsky et al. 2019, 2020) point out that temperature distributions are changing with global warming. The probability distribution function (PDF) of temperature is important for the frequency of weather extremes and their response to climate change (Huybers et al. 2014; Loikith and Neelin 2015; Ruff and Neelin 2012). Although in some cases the changes in global temperature extremes are well explained by a simple shift of the mean value (Rhines and Huybers 2013), the potential role of different moments of temperature PDFs on extreme events has recently garnered greater attention (Alexander and Perkins 2013; Garfinkel and Harnik 2017; Gao et al. 2015; Schneider et al. 2015).

Due to the severe impact of extreme temperature events on society and their potential change of frequency (Loikith and Neelin 2019; Wang et al. 2017; Sheridan and Lee 2018), especially for the increasing probability for anomalous heat events during summer in a warming climate (Perkins 2015), understanding of the physics behind the shape of temperature PDF needs to be improved (Hoskins and Woollings 2015). To that end, recent work has approached this question from a variety of perspectives. Garfinkel and Harnik (2017) demonstrated the role of horizontal temperature advection in generating non-Gaussianity in a simple Lagrangian model. Consistent with their finding, Linz et al. (2018) showed that similar skewness could be generated in a globally 2D idealized model where temperature is advected as a passive tracer stirred by stochastic Rossby waves. Employing a Lagrangian feature tracking algorithm, Tamarin-Brodsky et al. (2019) explored the effect of warm and cold anomalies in shaping temperature PDFs and explored how different physical processes related to these anomalous weather systems influence temperature variability in the Southern Hemisphere. The Lagrangian perspective has been further applied to study Northern Hemisphere temperature variability in Tamarin-Brodsky et al. (2020) and a simple theory on how temperature variance and skewness changes are generated dynamically from mean temperature gradient changes was developed.

Denotes content that is immediately available upon publication as open access.

Supplemental information related to this paper is available at the Journals Online website: https://doi.org/10.1175/JCLI-D-20-0920.s1.

Corresponding author: B. Zhang, boerzhang@g.harvard.edu

DOI: 10.1175/JCLI-D-20-0920.1

As advances have been made in linking regional and global temperature PDFs to large-scale meteorological patterns (Grotjahn et al. 2015; Loikith and Neelin 2019; Nakamura and Huang 2018) and the associated horizontal temperature advection as discussed above, some studies identified a variety of factors controlling certain tails of temperature PDFs. For example, in recent heatwave studies focusing on the warm tail of temperature PDFs (Bieli et al. 2015; Buzan and Huber 2020; Horton et al. 2016; Quinting and Reeder 2017; Zschenderlein et al. 2019), heatwaves in different regions have been attributed to a combination of horizontal temperature advection, radiation, surface heat fluxes, moist heat process, and subsidence. A wide spectrum of mechanisms—for example, soil moisture feedbacks (Seneviratne et al. 2010), quasi-resonant amplification of planetary waves (Petoukhov et al. 2013), large-scale orography (Lutsko et al. 2019), and Arctic warming (Barnes and Screen 2015; Coumou et al. 2015, 2018; Screen 2014)—also have the potential to influence temperature PDFs and their future change.

Due to the variety of controlling factors, local-level knowledge of the physical processes responsible for setting the shape of the temperature PDF remains unclear. In other words, how do different physical mechanisms quantitatively affect a certain percentile of the temperature PDF at a certain location? To answer this question, Linz et al. (2020) put forward a conditional mean framework quantifying the balance between large-scale temperature advection and all other processes in setting the shape of the temperature PDF. They demonstrated the effectiveness of the framework in examining and explaining the changing shapes of temperature PDFs in the midlatitudes in an idealized aquaplanet model and found that in midlatitudes the shape of temperature PDFs could largely be explained by horizontal temperature advection while parameterizing all the other processes with a simple Newtonian relaxation. Essentially, horizontal temperature advection acts to amplify perturbations from the mean while other processes act to damp perturbations from the mean. The Eulerian essence of this conditional mean framework also enables ready decomposition of the global horizontal advection field into stationary and transient terms, so as to resolve how different components of temperature gradient and circulation pattern explain temperature PDFs as a function of temperature percentiles. While this framework leads to interesting results with an idealized model, it is natural to ask, "What happens in the real world?". After all, the extreme events on land may have wider impacts than the ocean situation simulated in the idealized aquaplanet model, and different processes, like land–atmosphere interactions, zonally asymmetric land regions, and large-scale orography, will give more complexity to the physical processes controlling the shape of temperature PDFs. As such, it is unclear whether there are any regions that could be simply explained by horizontal temperature advection.

In this paper, we employ the same conditional mean framework as in Linz et al. (2020) to investigate how well the simplified linear relationship between horizontal temperature advection and the shape of the daily temperature PDF holds in the ERA5 data. We concentrate on 850 hPa rather than the surface, as this height has been commonly used in previous studies (Garfinkel and Harnik 2017; Schneider et al. 2015; Tamarin-Brodsky et al. 2019, 2020) and has been shown to be a good representation of near-surface extreme temperature events (Tamarin-Brodsky et al. 2020). We decompose horizontal advection into mean and transient terms to understand the dominant factors affecting different moments of temperature PDFs. Furthermore, we look beyond the simple framework to also perform a cursory examination the role of vertical processes (vertical advection and adiabatic processes) and diabatic processes in driving the shape of temperature PDFs on land.

The paper is organized as follows. In section 2, the data and methods are introduced. We applied the conditional mean framework to ERA5 data and present those results in section 3. Section 4 describes the effects of different transient and stationary components of horizontal temperature advection in shaping temperature variance and skewness in the context of the conditional mean framework. In section 5, we focus on PDFs over land, using clustering analysis to identify different regions according to the balance between conditional mean temperature advection and other processes in shaping the temperature PDF. Limitations of this study, a summary, and conclusions are discussed in section 6.

2. Data and methods

a. Conditional mean framework

The conditional mean framework we are using to explain temperature PDFs closely follows Linz et al. (2020), where it effectively explained the midlatitude temperature PDFs in an idealized aquaplanet model. Similar methods have also been used to study extreme precipitation (Chen et al. 2019; Ma et al. 2020; Norris et al. 2019a,b). For completeness, a description of it follows.

The temperature (T) tendency at a certain location can be described by

$$\frac{\partial T}{\partial t} = -\mathbf{v}\cdot\nabla T - \omega\frac{\partial T}{\partial p} + \dot{T}, \tag{1}$$

where $\mathbf{v}$ is the horizontal wind vector, (u, v), ∇T is the horizontal temperature gradient, ω is vertical velocity in pressure, $\partial T/\partial p$ is temperature gradient with pressure, and $\dot{T}$ is the total derivative of temperature, which could be interpreted as the influence of other processes like adiabatic processes, radiation, and latent heat release. Note that in Linz et al. (2020), the authors are using potential temperature θ when introducing the theory, but are applying the theory to temperature when conducting their analysis. To avoid any confusion, we choose to directly introduce the theory in terms of temperature T. It is also worth pointing out that on a constant pressure surface (850 hPa here), temperature and potential temperature differ only by a constant: $\theta = T(1000/850)^{R/c_p}$. It can also be proved that the vertical advection of potential temperature $-\omega\partial\theta/\partial t$ equals the vertical transport term $\langle\omega(\kappa T/p - \partial T/\partial p)\rangle_{T^e}$ of temperature, which is going to be

further discussed in our section 5. The derivation in the current study is equivalent to the version in Linz et al. (2020). We choose to write a first-order Taylor approximation of $\dot{T}$ as

$$\dot{T} \approx -\frac{T - T_{\mathrm{eq}}}{\tau}, \tag{2}$$

which can be interpreted as a linear Newtonian relaxation process toward a equilibrium temperature T_{eq} with a characteristic time of τ. Using this approximation and also absorbing the vertical part of temperature advection $-\omega\partial T/\partial p$ into the $\dot{T}$ term, (we will examine this assumption in sections 3 and 5), Eq. (1) can be idealized as a combination of horizontal advection driving the temperature tendency and a relaxation term caused by all the other processes:

$$\frac{\partial T}{\partial t} = -\mathbf{v}\cdot\nabla T - \frac{T - T_{\mathrm{eq}}}{\tau}. \tag{3}$$

An explanatory equation for temperature PDFs is derived from Eq. (3) through calculating the conditional mean on the percentile of temperature, that is,

$$\left\langle \frac{\partial T}{\partial t} \right\rangle_{T^e} = \langle -\mathbf{v}\cdot\nabla T\rangle_{T^e} - \frac{\langle T\rangle_{T^e} - T_{\mathrm{eq}}}{\tau}. \tag{4}$$

Here, $\langle X\rangle_{T^e}$ means the conditional mean of variable X at the temperature PDF percentile e. Linz et al. (2020) show in their Eqs. (3)–(6) that $\langle \partial T/\partial t\rangle_{T^e}$ is equal to the trend of the temperature at a certain percentile T^e: $\langle \partial T/\partial t\rangle_{T^e} = \partial T^e/\partial t$. We also find that the temperature tendency vanishes when conditionally averaged at each temperature percentile, since the accumulation of temperature tendency at a fixed temperature percentile over a long period will be negligible, if the long-term trend is small. We inspect the long-term trend at 49 evenly distributed percentiles (2nd, 4th, …, 98th) using quantile regression (e.g., Koenker and Bassett 1978; Cade and Noon 2003) and find that the magnitude of largest trend among all the grid points and percentiles is smaller than 0.1 K yr^{-1}, or 3.2×10^{-9} K s^{-1}, while a typical magnitude of the conditional mean of horizontal temperature advection is about $\times 10^{-5}$ K s^{-1} (e.g., Fig. 2d; see movie S1 in the online supplemental material). Thus we can safely ignore the LHS of Eq. (4). (Note that we are not claiming that the trend in temperature is negligible, but we are justifying that it is reasonable to treat the period of study, 1979–2019, as a single climate state in our current analysis and to ignore the LHS.) Then we have

$$T^e = \tau\cdot\langle -\mathbf{v}\cdot\nabla T\rangle_{T^e} + T_{\mathrm{eq}}, \tag{5}$$

where T^e is the temperature at the eth percentile, $T^e = \langle T\rangle_{T^e}$. Equation (5) states that the temperature at a particular percentile can be linearly related to the conditional mean of horizontal temperature advection at that temperature percentile. Hereafter, this conditional average of temperature advection term will be referred to as "conditional temperature advection" following Linz et al. (2020). If observations exhibit a linear relationship between temperature and conditional temperature advection, we can interpret the slope of the linear relationship as τ and the intercept as T_{eq}. Significant deviations from this linear relationship indicate the importance of processes other than conditional temperature advection in explaining the shape of the temperature distribution. Generally, τ and T_{eq} need not be independent of the percentile. If the first-order Taylor expansion [Eq. (2)] is effective with the same or nearly the same τ and T_{eq} over the full distribution, however, the temperature distribution would be explained by conditional temperature advection. That is to say that if other processes always act as a damping effect, they cannot explain any movement of the temperature away from the mean. Constant coefficients worked surprisingly well in the idealized simulation reported in Linz et al. (2020) and will be examined with reanalysis data in section 3.

When evaluating the conditional mean of temperature T^e and conditional temperature advection $\langle -\mathbf{v}\cdot\nabla T\rangle_{T^e}$, we divide the temperature PDF evenly into M percentile bins:

$$e_i = \frac{100i}{M+1}, i = 1, ..., M. \tag{6}$$

The conditional mean value at the e_ith temperature percentile is evaluated as the average over the temperature percentile range of $[e_{i-0.5}, e_{i+0.5}]$ rather than just the event at the e_ith percentile so as to acquire a relatively smooth distribution function. It is interesting to point out that the premise behind our conditional mean framework is the same as standard composite methods: we are actually compositing horizontal temperature advection into different bins according the percentile of temperature in order to see what is important for temperature in that bin. In this paper, M is chosen as 49 to strike a balance between the resolution of temperature PDF and a large enough sample size to achieve reliable average values. Other M values such as 19, 199, and 499 have also been studied (not shown here) and do not qualitatively change the results.

In sections 3 and 5, we apply a "local normalization" to the conditional temperature advection $\langle -\mathbf{v}\cdot\nabla T\rangle_{T^e}$ or percentile mean temperature T^e. If there is no further specification, we normalize the 49-point-vector of conditional temperature advection or the 49-point-vector of percentile mean temperature at each grid point by first subtracting the mean and then dividing by the standard deviation of the 49 values at that grid point.

b. *ERA5 data*

The data used for this study come from the ERA5 dataset (Hersbach et al. 2020) produced by the European Centre for Medium-Range Weather Forecasts (ECMWF). We use data at 850-hPa level during 1979–2019, for temperature, horizontal wind, and vertical velocity (ω) fields. Temperature data at 825 and 875 hPa are also used when calculating the vertical temperature gradient. Both JJA and DJF seasons are studied. We use data at 0000, 0600, 1200, and 1800 UTC and average them for each day to obtain the daily data for both temperature and advection data (derived from wind and temperature fields). The raw daily data are used and no climatology is subtracted considering that we are studying the original PDF of temperature. We use the resolution of 0.25° × 0.25° when

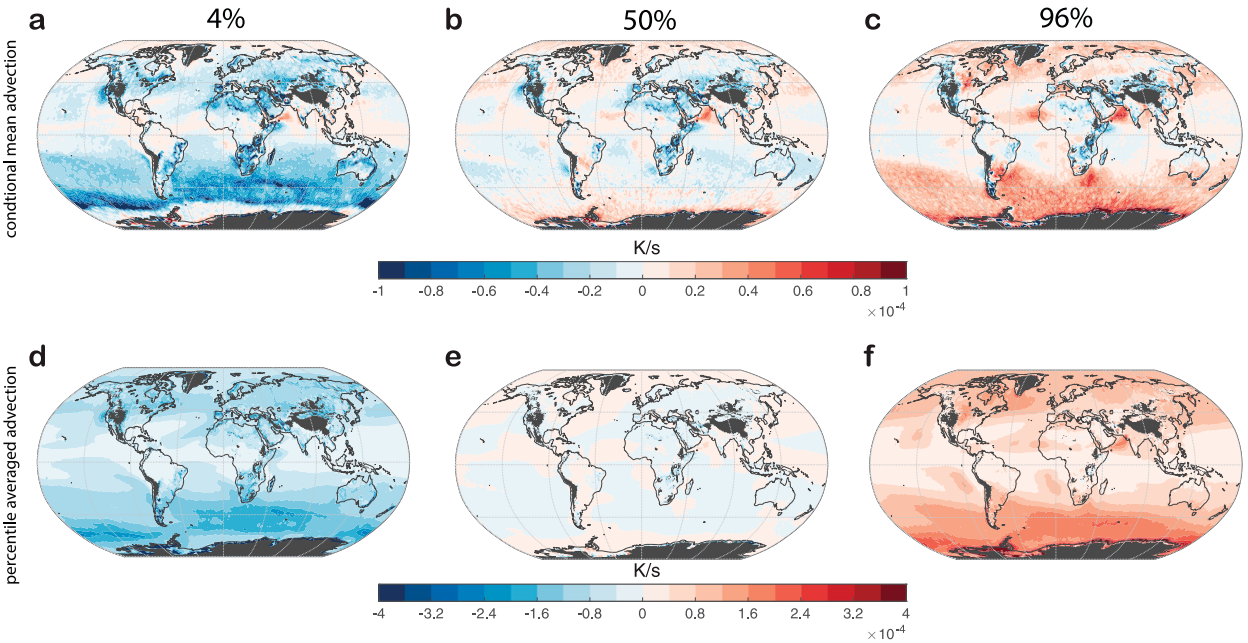

FIG. 1. 850-hPA JJA (a)–(c) conditional temperature advection $\langle -\mathbf{v}\cdot\nabla T\rangle_{T^e}$ (K s^{-1}) and (d)–(f) percentile mean of temperature advection $\langle -\mathbf{v}\cdot\nabla T\rangle_{(-\mathbf{v}\cdot\nabla T)^e}$ (K s^{-1}) patterns based on ERA5 data over years 1979–2019 across different percentiles: (a),(d), 4th percentile, (b),(e), 50th percentile, and (c),(f), 96th percentile.

conducting all calculations like computing temperature gradient; however, we present the data in all figures using a resolution of 1.25° × 1.25°, by only picking a subset of the data. Considering that some of the grid points will be under terrain at certain points for 850 hPa, which will make the results less meaningful, we choose to mask the grid points with land height higher than 1400 m.

3. Linear fitting: The first-order approximation for temperature PDFs

The conditional mean temperature advection $\langle -\mathbf{v}\cdot\nabla T\rangle_{T^e}$ and the percentile mean of advection itself [denoted as $\langle -\mathbf{v}\cdot\nabla T\rangle_{(-\mathbf{v}\cdot\nabla T)^e}$] at 850 hPa for ERA5 data are separately calculated to look at the conditional mean framework. Figures 1a–c show the changes of conditional temperature advection $\langle -\mathbf{v}\cdot\nabla T\rangle_{T^e}$ across three different percentiles (4%, 50%, 96%) during JJA. As we mentioned in section 2a, the conditional mean of horizontal temperature advection could be understood as a composite of the corresponding horizontal advection when the temperature are in bins of certain ranges (here the bins are 3%–5%, 49%–51%, and 95%–97%, respectively, of the whole temperature time series at each grid point). Above most of the mid- to high-latitude oceans in both hemispheres, there is clearly an increase in conditional temperature advection when the percentile of temperature increases, which means that the conditional horizontal temperature advection is positively correlated with the temperature distribution at these grid points. (Note that there could be negative values of conditional temperature advection, so an increase could involve changing from a negative value to a positive value.) This is surprising because we can expect that above mid- to high-latitude oceans the temperature advection should be a major contributor to the temperature distribution at each grid point. On the other hand, the relationship does not perfectly hold true above tropical regions and over the land, which means the relationships between advection and temperature distributions could be more complex. Figures 1d–f show the percentile mean of temperature advection $\langle -\mathbf{v}\cdot\nabla T\rangle_{(-\mathbf{v}\cdot\nabla T)^e}$ across the same three percentiles, which reflects the character of horizontal advection itself. The value of $\langle -\mathbf{v}\cdot\nabla T\rangle_{(-\mathbf{v}\cdot\nabla T)^e}$ is directly calculated at each grid point by first sorting the whole temperature time series and then take averages in 2-percentile bins near the percentiles we are focusing on (here the bins of temperature advection being averaged are 3%–5%, 49%–51%, and 95%–97%, respectively). We are showing Figs. 1d–f to stress that the conditional mean temperature advection in Figs. 1a–c is not the same as the distributions of advection itself. By definition, the percentile average advection $\langle -\mathbf{v}\cdot\nabla T\rangle_{(-\mathbf{v}\cdot\nabla T)^e}$ increases monotonically with the advection percentile. As we expected, the conditional temperature advection $\langle -\mathbf{v}\cdot\nabla T\rangle_{T^e}$ (Figs. 1a–c) does not have any obvious relationship with the PDF of temperature advection itself $\langle -\mathbf{v}\cdot\nabla T\rangle_{(-\mathbf{v}\cdot\nabla T)^e}$ (Figs. 1d–f).

A reduced major axis (RMA; e.g., Smith 2009) linear regression is applied to 850-hPa JJA global percentile temperature mean and conditional temperature advection with M = 49 different temperature percentiles (as described in section 2) at each grid point to inspect the relationship in Eq. (5). Figure 2a shows the Pearson correlation coefficient of the

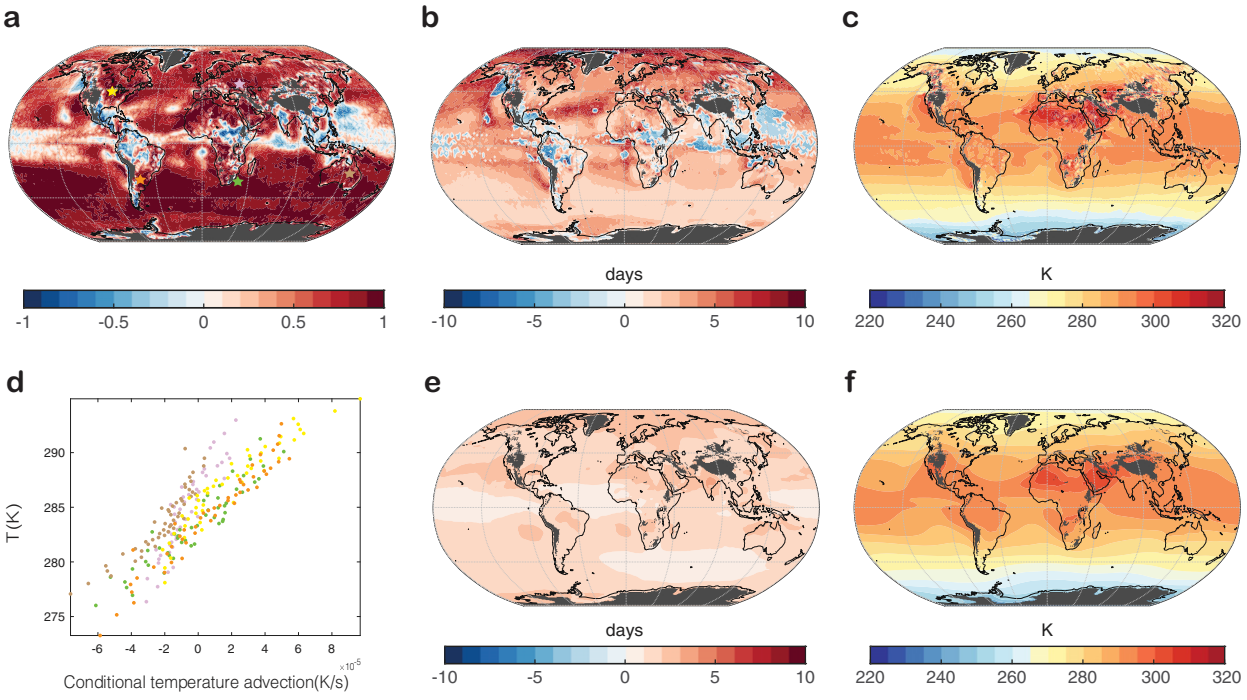

FIG. 2. (a)–(c) Reduced major axis linear regression results between 850-hPa JJA conditional temperature advection and temperature based on ERA5 data. (a) Linear Pearson correlation coefficient r value. The stars shows locations chosen in (d). (b) Slope of linear fit: relaxation time scale τ (days). (c) Intercept of linear fit: equilibrium temperature T_{eq} (K). (d) The scatterplots between temperature at different percentiles T^e and conditional mean temperature advection $\langle -\mathbf{v}\cdot\nabla T\rangle_{T^e}$ at the locations shown in (a). Colors of the points in the scatterplots in (d) are chosen to be the same as colors of stars showing corresponding locations in (a). (e) The e-folding time scale of the autocorrelation function for temperature time series at 850 hPa in JJA during 1979–2019 based on ERA5 data, τ_{ac} in days. (f) Time-averaged temperature in K calculated from temperature time series at 850 hPa in JJA during 1979–2019.

linear regression. Note that the regression itself is a test on where conditional advection can explain the temperature distribution linearly. Where r is high, the relationship in Eq. (5) as well as the Taylor expansion in Eq. (2) work well across all percentiles; when r is not high or even negative, other processes (e.g., adiabatic processes, radiation, and latent heat release) have different effects at different percentiles, suggesting that they are critical for shaping the distribution. In Fig. 2a there is a consistently high positive r pattern over a large fraction of the globe, especially above the mid- to high latitudes in the Northern Hemisphere and Southern Hemisphere ocean. A visualization of the relationships between JJA temperature and conditional temperature advection over different latitudes, and also the difference between land and ocean, is shown in Fig. 3, where locally normalized conditional temperature advection and locally normalized conditional average temperature are aggregated in different regions and shown in grid-cell-area-weighted scatterplots. (When calculating the grid-cell-area-weighted densities, we use 100×100 bins for each panel, and for each bin we calculate the sum of the total areas of all grid cells where all the points in that bin come from. Then the results are normalized by the size of the bin to ensure that the densities are independent from the scales of the bin. Thus, the units of the color bars are square meters.) The difference between the top and bottom rows of Fig. 3 shows that the linear relationship between temperature and conditional temperature advection is better over the mid- to high latitudes than over the tropics, which is true both above ocean and land. The difference between the left and right columns of Fig. 3 shows that the linearity is better above ocean than above land. To demonstrate that the high r value reflects a truly linear relationship between temperature and conditional temperature advection, temperatures at different percentiles are plotted against conditional temperature advection in Fig. 2d at certain locations marked as stars in Fig. 2a, and there is no obvious deviation from linear where the fit is quite good. However, certain areas with negative r values also exist, which means that the simple uniform relaxation across all temperature percentiles in Eq. (5) unsurprisingly does not capture the complete physics of all the other processes shaping the temperature PDF. This is especially true in the tropics, where horizontal temperature advection is small. Near orography, the horizontal temperature advection is also not the dominant factor shaping the temperature distribution (e.g., in Patagonia). In section 5, we will further discuss the nonlinearity (i.e., the influence of other processes) in shaping temperature PDFs.

The relaxation time scale in Fig. 2b (obtained from the slope of the regression) has the same pattern in the sign, with the magnitude ranging from less than a day to more

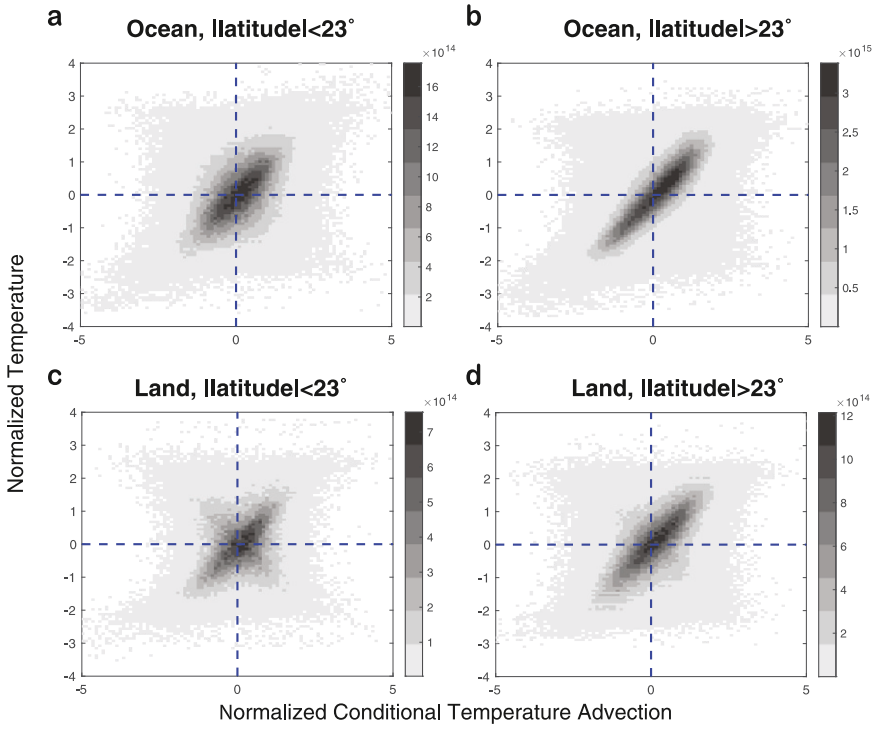

FIG. 3. A visualization for the difference of the relationships between temperature and conditional mean horizontal temperature advection over different regions. Scatterplots for locally normalized conditional temperature advection vs locally normalized conditional average temperature with shading showing the grid-cell-area-weighted density (m^2) of the points are plotted for different regions. All the percentiles are shown together in this figure. Results are shown for (a) above ocean, with the absolute value of latitude smaller than 23°; (b) above ocean, with the absolute value of latitude larger than 23°; (c) above land, with the absolute value of latitude smaller than 23°; and (d) above land, with the absolute value of latitude larger than 23°. The data are weighted by the area of the grid cells where the data come from, to reflect the difference of the size of the grid cells at different latitudes. Refer to the text for more details of the normalization, and the calculation of the grid-cell-area-weighted densities.

than a week, somewhat consistent with synoptic time scales. Figure 2c shows the equilibrium temperature obtained from the intercept of the regression. There is a meridional dependence of equilibrium temperature with higher values near the tropical region and lower values near the polar region. Land–sea contrast and patterns related to orography are also evident. A previous study found that the variance and skewness of midlatitude temperature PDF could be generated in an idealized model where temperature is advected nonlinearly as a passive tracer with a Newtonian relaxation to the equilibrium temperature (Linz et al. 2018), with a globally homogeneous relaxation time scale τ and zonally symmetric equilibrium temperature T_{eq}. The linear regression results in Figs. 2b and 2c demonstrate that what happens in the real world is largely in accordance with the idealized simulation, especially above midlatitude oceans.

The negative τ values are not at first intuitive, and hence we now explain how such a result comes about to explain this. At a given time and location, the temperature will of course fall in a certain percentile. The question is what will cause the temperature to change to a different percentile. This framework identifies where horizontal temperature advection acts to bring the temperature away from the mean toward more extreme values. Where the first-order Taylor expansion is appropriate and τ and T_{eq} are constant across percentiles, the combination of all the other processes act together to oppose deviations from the mean from developing into more extreme values in basically the same way at every percentile. Obviously these processes are still necessary for shaping the distribution, but their role does not vary at the 90th versus the 10th percentile—they are a simple linear damping. Where τ is negative, instead horizontal temperature advection is damping perturbations, and the other processes affecting temperature must compensate for this effect in order for the temperature to reach a more extreme percentile.

To avoid any confusion, we would like to emphasize that τ is not interchangeable with any natural physical time scale (such as the synoptic time scale or the radiative time scale)

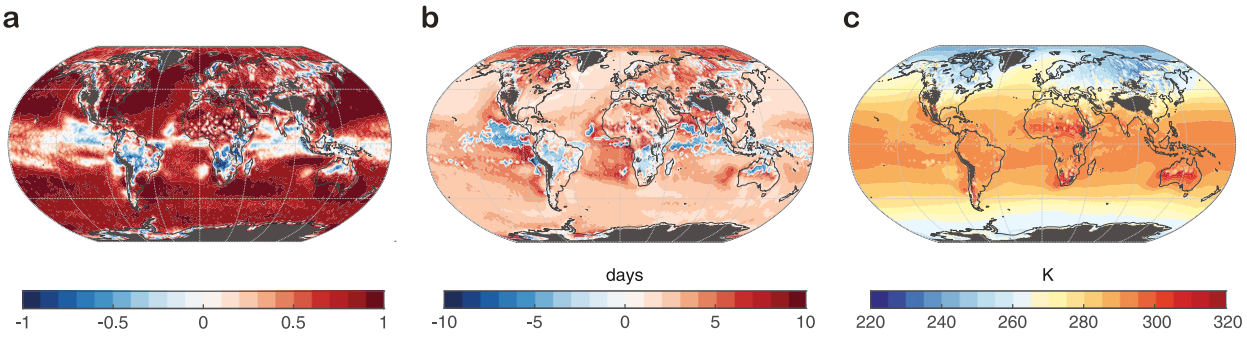

FIG. 4. Reduced major axis linear regression results between 850-hPa DJF conditional temperature advection and temperature distribution based on ERA5 data. (a) Linear correlation coefficient r value. (b) Slope of linear fit: relaxation time scale τ (days). (c) Intercept of linear fit: equilibrium temperature T_{eq} (K).

and T_{eq} is also not interchangeable with the time-averaged temperature. We demonstrate this more explicitly in Figs. 2e and 2f. To contrast between τ and the autocorrelation time scale of the temperature τ_{ac}, we show the spatial distribution of the e-folding autocorrelation time scale in Fig. 2e. To obtain that time scale, we calculated the autocorrelation coefficient separately for the JJA season in each year, with the time lag from 6 h to 25 days. After averaging all the seasonal autocorrelation functions from 1979 to 2019, we used nonlinear least squares fitting method on it to obtain the e-folding time scale. Although we can see similarity between the autocorrelation time scale τ_{ac} and the relaxation time scale τ under our conditional mean framework, the difference between these two variables is also significant. The spatial distribution of time-averaged temperature T_{mean} is shown in Fig. 2f. Similarities between T_{eq} and T_{mean} can also be observed (e.g., the high temperature region above Sahara Desert and on the west coast of North America), but significant differences also exist (e.g., the temperature patterns between T_{eq} and T_{mean} above tropical oceans are quite different). This comparison shows that the Newtonian relaxation parameterization is still simply a Taylor series expansion, and its coefficients are not readily interpretable as something more physically meaningful.

The same linear regression has also been applied to DJF daily data during 1979–2019, as shown in Fig. 4. Similar linear correlation coefficient r patterns as in JJA can be observed (Fig. 4a), although clear differences from JJA do exist, especially above tropical oceans. Generally r is higher in the Northern Hemisphere (especially above ocean) and lower in the Southern Hemisphere (especially above land) than in JJA, suggesting that temperature distributions are more directly related to conditional temperature advection in the winter hemisphere. Similar differences in the Newtonian relaxation time scale τ (Fig. 4b) can also be found, and τ is lower in the Northern Hemisphere and higher in the Southern Hemisphere than in JJA. The equilibrium temperature T_{eq} (Fig. 4) also reflects seasonal differences between JJA and DJF, with a lower equilibrium temperature in the winter hemisphere and higher equilibrium temperature in the summer hemisphere. Since the conditional mean framework is effective in explaining the relationship between temperature and conditional temperature advection, in the mid- to high latitudes, in the next section we focus on the role of different transient and stationary components in shaping different moments of temperature PDF, which has been a topic of interest in recent studies (Garfinkel and Harnik 2017; Linz et al. 2018; Tamarin-Brodsky et al. 2019).

4. How do different components of temperature advection influence the variance and skewness of temperature PDFs?

The horizontal temperature advection can decomposed into transient and stationary terms as follows:

$$-\mathbf{v}\cdot\nabla T = -\bar{\mathbf{v}}\cdot\nabla\bar{T} - \mathbf{v}'\cdot\nabla\bar{T} - \bar{\mathbf{v}}\cdot\nabla T' - \mathbf{v}'\cdot\nabla T'. \quad (7)$$

Here, $\bar{X}$ is the monthly average of variable X (i.e., the stationary part) and $X' = X - \bar{X}$ is the transient part. When performing the monthly average, we separately calculate a mean value for each calendar month, and subtract it from that month's data to get X'. A few studies claim that temperature standard deviation can be linked to $-\mathbf{v}'\cdot\nabla\bar{T}$ (i.e., anomalous advection of the background stationary temperature gradient), while the contribution of other terms is insignificant (Schneider et al. 2015; Linz et al. 2018; Tamarin-Brodsky et al. 2019). Meanwhile, the nonlinear transient term, $-\mathbf{v}'\cdot\nabla T'$, has been shown to be critical for temperature skewness in the Southern Hemisphere or zonally symmetric models (Garfinkel and Harnik 2017; Linz et al. 2018; Tamarin-Brodsky et al. 2019). To our best knowledge, the influence of horizontal temperature advection on further higher-order moments (e.g., kurtosis) has not been studied.

To quantify the influence of conditional advection on different moments of temperature, we use the following approximate equations based on the conditional mean method and inspired by Tamarin-Brodsky et al. (2020). We define $(-\mathbf{v}\cdot\nabla T)_{w0}$ as the warmer part of the horizontal temperature advection $-\mathbf{v}\cdot\nabla T$ (i.e., the mean value of temperature advection on the condition that temperature T is larger than its mean value) and define $(-\mathbf{v}\cdot\nabla T)_{c0}$ as the colder part of the horizontal temperature advection $-\mathbf{v}\cdot\nabla T$ (i.e., the mean value of temperature advection on the condition that

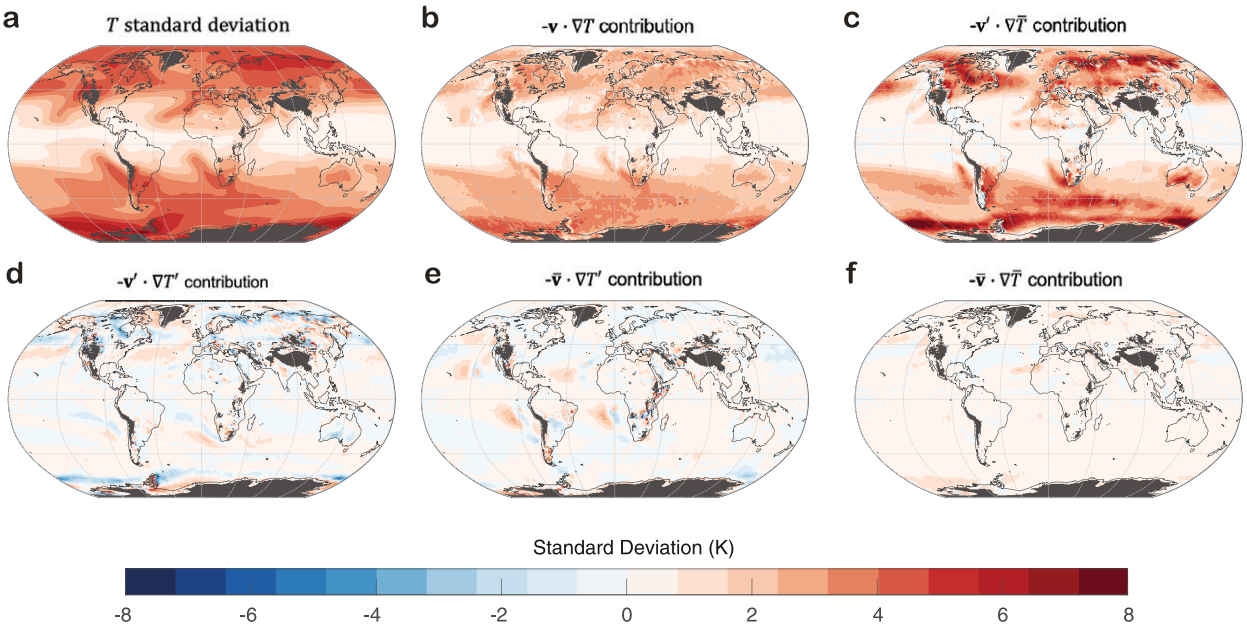

FIG. 5. 850-hPa JJA temperature standard deviation and influences of different advection components on it. (a) Temperature standard deviation (K), (b) approximate influence of horizontal temperature advection on temperature standard deviation $\tau \times (1/2) \times [(-\mathbf{v} \cdot \nabla T)_w + (-\mathbf{v} \cdot \nabla T)_c]$ (K) [the pattern correlation with (a) is 0.86], and contributions of the four components: (c) anomalous advection of stationary temperature gradient $\tau \times (1/2) \times [(-\mathbf{v}' \cdot \nabla \bar{T})_w + (-\mathbf{v}' \cdot \nabla \bar{T})_c]$ (K), (d) covariance between anomalous wind and anomalous temperature $\tau \times (1/2) \times [(-\mathbf{v}' \cdot \nabla T')_w + (-\mathbf{v}' \cdot \nabla T')_c]$ (K), (e) stationary advection of anomalous temperature gradient $\tau \times (1/2) \times [(-\bar{\mathbf{v}} \cdot \nabla T')_w + (-\bar{\mathbf{v}} \cdot \nabla T')_c]$ (K), and (f) stationary advection of stationary temperature gradient $\tau \times (1/2) \times [(-\bar{\mathbf{v}} \cdot \nabla \bar{T})_w + (-\bar{\mathbf{v}} \cdot \nabla \bar{T})_c]$ (K).

temperature T is smaller than its mean value); we also define $(-\mathbf{v} \cdot \nabla T)_{\bar{T}}$ as the value of horizontal temperature advection on the condition that the temperature is exactly at its mean value. If we also define $(-\mathbf{v} \cdot \nabla T)_w = (-\mathbf{v} \cdot \nabla T)_{w0} - (-\mathbf{v} \cdot \nabla T)_{\bar{T}}$, the amplitude of the mean horizontal temperature advection contributing to the warmer part of the temperature PDF. Likewise, we define $(-\mathbf{v} \cdot \nabla T)_c = (-\mathbf{v} \cdot \nabla T)_{\bar{T}} - (-\mathbf{v} \cdot \nabla T)_{c0}$, the amplitude of the mean horizontal temperature advection contributing to the colder part of the temperature PDF. The contribution of horizontal advection to temperature variance and skewness can be estimated as

$$\sigma_{-\mathbf{v} \cdot \nabla T} = \frac{1}{2} \times \tau \times [(-\mathbf{v} \cdot \nabla T)_w + (-\mathbf{v} \cdot \nabla T)_c] \tag{8}$$

and

$$S_{-\mathbf{v} \cdot \nabla T} = \frac{\tau \times [(-\mathbf{v} \cdot \nabla T)_w - (-\mathbf{v} \cdot \nabla T)_c]}{\sigma_T}, \tag{9}$$

respectively, where τ is the same relaxation time scale, and σ_T is the real standard deviation of temperature time series. A more detailed explanation of these two equations can be found in the appendix. Our equations are totally based on the simplified expressions for variance and skewness in Tamarin-Brodsky et al. (2020), where they are using the absolute average intensities of warm and cold anomalies identified from their Lagrangian feature tracking method to estimate the variance and skewness of temperature. Note that in Tamarin-Brodsky et al. (2020) the intensities of warm and cold anomalies and are always positive, whereas our $(-\mathbf{v} \cdot \nabla T)_w$ and $(-\mathbf{v} \cdot \nabla T)_c$ here could have negative values where the correlations between conditional advection and temperature are low. Since Eqs. (8) and (9) are linear functions of conditional temperature advection $-\mathbf{v} \cdot \nabla T$, they can also be directly applied to the four different stationary and transient components of conditional temperature advection shown in Eq. (7) to get the contribution of these different terms to variance and skewness of temperature PDFs.

We test the validity of these approximations, and these results are shown in Figs. 5a,b (JJA) and Figs. 7a,b (DJF) (standard deviation) and Figs. 6a,b (JJA) and Figs. 8a,b (DJF) (skewness). We do not expect exact agreement between the true temperature standard deviation or skewness and the ones calculated in this way for two main reasons: First, the linear relationship between temperature and temperature advection holds best only in midlatitudes; Eqs. (8) and (9) assume this linear relationship is always good [we are essentially using the linear regression Eq. (5) to estimate the contribution of advection to temperature distributions]. Second, in our estimation we are using only a single value for the warmer part of the distribution, and a single value for the colder part of the distribution, to estimate the standard deviation, thus implicitly assuming a two-point distribution in the derivation of the method. This is an assumption made for

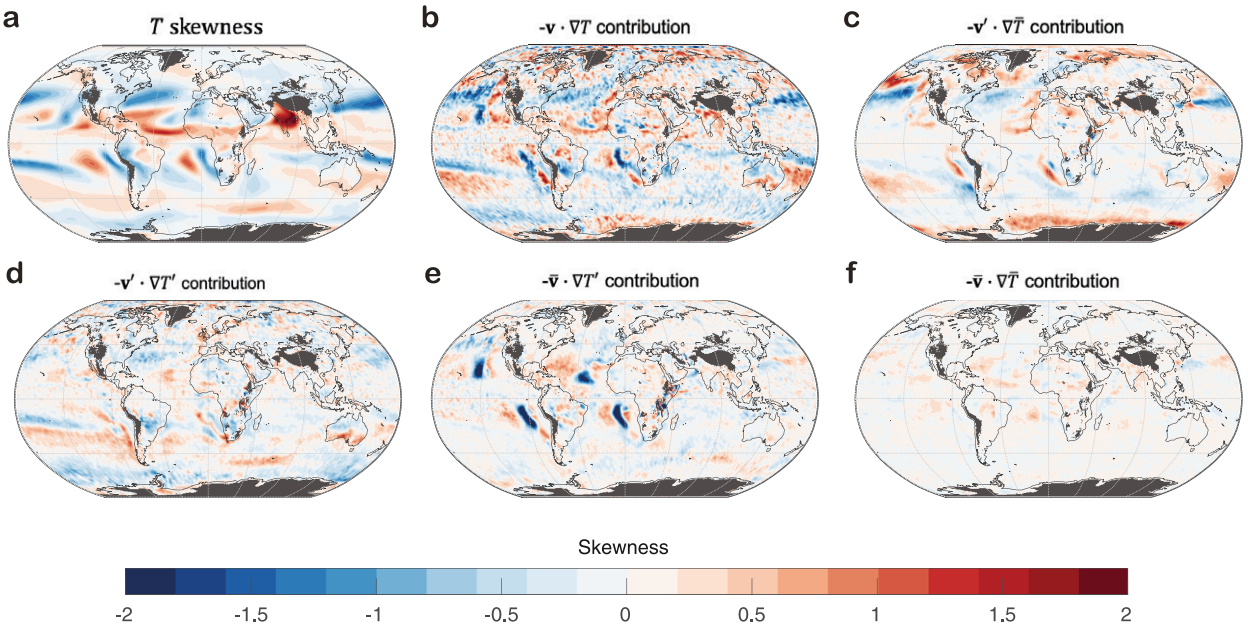

FIG. 6. 850-hPa JJA temperature skewness and influences of different horizontal temperature advection components on it: (a) temperature skewness, (b) approximate influence of advection on temperature skewness $\{\tau\times[(-\mathbf{v}\cdot\nabla T)_w-(-\mathbf{v}\cdot\nabla T)_c]\}/\sigma_T$ [the pattern correlation with (a) is 0.36], and contributions of the four components: (c) anomalous advection of stationary temperature gradient $\{\tau\times[(-\mathbf{v}'\cdot\nabla\bar{T})_w-(-\mathbf{v}'\cdot\nabla\bar{T})_c]\}/\sigma_T$, (d) covariance between anomalous wind and anomalous temperature $\{\tau\times[(-\mathbf{v}'\cdot\nabla T')_w-(-\mathbf{v}'\cdot\nabla T')_c]\}/\sigma_T$, (e) anomalous advection of stationary temperature gradient $\{\tau\times[(-\bar{\mathbf{v}}\cdot\nabla T')_w-(-\bar{\mathbf{v}}\cdot\nabla T')_c]\}/\sigma_T$, and (f) stationary advection of stationary temperature gradient $\{\tau\times[(-\bar{\mathbf{v}}\cdot\nabla\bar{T})_w-(-\bar{\mathbf{v}}\cdot\nabla\bar{T})_c]\}/\sigma_T$. Note that (b)–(f) are smoothed by calculating the mean value of all the neighboring grid points in the 1.75° × 1.75° areas.

simplicity but the actual distribution is obviously not a two-point distribution. [See our appendix, and also supplementary information section 2 of Tamarin-Brodsky et al. (2020)]. Figure 5a (JJA) and Fig. 7a (DJF) show the true standard deviation of 850-hPa temperature, and Fig. 5b (JJA) and Fig. 7b (DJF) show the approximate contribution of horizontal temperature advection to temperature standard deviation calculated from the conditional temperature advection using Eq. (8). The spatial pattern of the approximate contribution of temperature advection to the temperature standard deviation is similar to the pattern of the real temperature standard deviation, but the magnitude of the former is smaller. This is likely due to our approximation method, as was just mentioned. For the approximate contribution of 850-hPa horizontal temperature advection to temperature skewness, the results are somewhat noisy (e.g., the JJA result without smoothing is shown in Fig. S1), mainly due to small-scale disturbances related to anomalous temperature gradient $\nabla T'$ (e.g., Figs. S1c,d for JJA). Thus we smoothed the results for both JJA and DJF spatially by using a 1.75° × 1.75° simple moving average, and the results are shown in Fig. 6 (JJA) and Fig. 8 (DJF). The approximate skewness contribution of conditional temperature advection calculated by the approximate method [Fig. 6b (JJA) and Fig. 8b (DJF)] also captures the spatial pattern of temperature skewness [Fig. 6a (JJA) and Fig. 8a (DJF)]. The consistency between the moments calculated directly from temperature and those calculated using the linear approximations based on conditional temperature advection gives us further confidence in applying the conditional mean framework to study the influence of advection on temperature PDFs.

Recall that previous studies showed that the anomalous advection of the stationary temperature gradient was key in determining the standard deviation of temperature distributions (Schneider et al. 2015; Garfinkel and Harnik 2017; Linz et al. 2018; Tamarin-Brodsky et al. 2019). In Figs. 5c–f (JJA) and Figs. 7c–f (DJF), we show the breakdown between the different stationary and transient components, and we also find that $-\mathbf{v}'\cdot\nabla\bar{T}$ is the most important. Note that the different stationary and transient components of temperature advection can have negative contributions to the temperature standard deviation, for example, when the relaxation time scale τ value from the linear regression Eq. (5) is positive, but the conditional means of a component of temperature advection have a higher value when temperature is higher than its mean value (the warmer part), and a lower value when temperature is lower than its mean value [the colder part; see our Eq. (8)]. For the two terms related to anomalous temperature gradient $-\bar{\mathbf{v}}\cdot\nabla T'$ [Fig. 5d (JJA) and Fig. 7d (DJF)] and $-\mathbf{v}'\cdot\nabla T'$ [Fig. 5e (JJA) and Fig. 7e (DJF)], the same patterns do exist, but the overall contributions are relatively small. The contribution of the stationary term $\bar{\mathbf{v}}\cdot\nabla\bar{T}$ [Fig. 5f (JJA) and Fig. 7f (DJF)] is almost negligible, as expected.

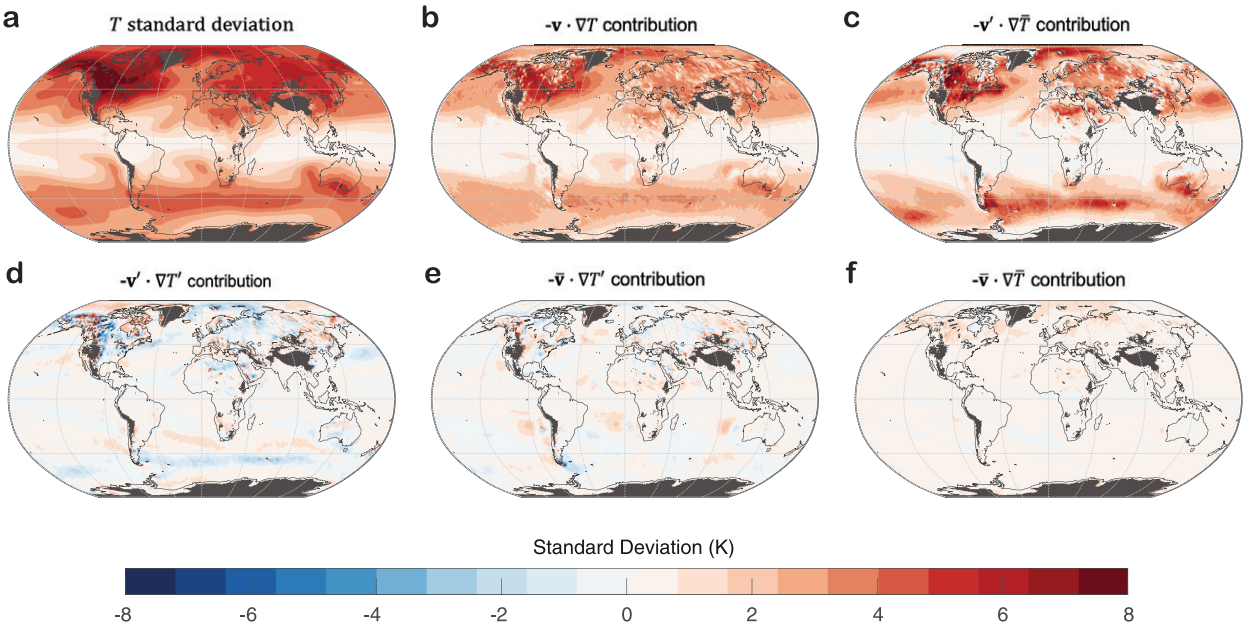

FIG. 7. As in Fig. 5, but for DJF. The pattern correlation between (a) and (b) is 0.87.

Our result for the different contributions of stationary and transient terms to the skewness [Figs. 6c–f (JJA) and Figs. 8c–f (DJF)] is somewhat more unexpected. We find that both the $-\mathbf{v}' \cdot \nabla \bar{T}$ [Fig. 6c (JJA) and Fig. 8c (DJF)] and $-\mathbf{v}' \cdot \nabla T'$ [Fig. 6d (JJA) and Fig. 8d (DJF)] terms contribute significantly to the spatial pattern of the full advection term [Fig. 6 (JJA) and Fig. 8 (DJF)]. As opposed to situations with zonally symmetric temperature gradients focused upon (Garfinkel and Harnik 2017; Linz et al. 2018; Tamarin-Brodsky et al. 2019), our result shows that although $-\mathbf{v}' \cdot \nabla T'$ contributes to the skewness pattern, the temperature advection by anomalous transport of the stationary temperature gradient $-\mathbf{v}' \cdot \nabla \bar{T}$ plays an even more important role. The other two terms [Fig. 6e,f (JJA) and Figs. 8e,f (DJF)] do not have very clear large-scale patterns, although $-\bar{\mathbf{v}} \cdot \nabla T'$ has relatively large values in certain regions (e.g., off the west coast of continents).

The fact that the linear advection term $-\mathbf{v}' \cdot \nabla \bar{T}$ also contributes to temperature skewness significantly is an interesting result. Although it has been shown that with a zonally symmetric background temperature gradient the linear advection $-\mathbf{v}' \cdot \nabla \bar{T}$ term could not generate temperature skewness (Garfinkel and Harnik 2017; Linz et al. 2018), the temperature gradient configuration in the real world could still lead to significant contribution of the $-\mathbf{v}' \cdot \nabla \bar{T}$ term to skewness. This result also supports Tamarin-Brodsky et al.'s (2020) [see their equation for skewness between their Eqs. (2) and (3)] and Garfinkel and Harnik's (2017) (see their second item in their section 6a) arguments that the linear advection term could be important to skewness if meridionally asymmetric temperature gradient already exists. The land–sea contrast, large-scale orography, and general circulation in real climate can give complexity to the physics of temperature PDF. Considering that the anomalous advection of stationary temperature gradient term plays an important role in explaining both the standard deviation and skewness of temperature PDFs, we explore the role of its meridional component $-v'_y(\partial \bar{T}/\partial y)$ and zonal component $-v'_x(\partial \bar{T}/\partial x)$ separately in Fig. S2 (only JJA data are analyzed as an example here). We find that compared to the zonal component $-v'_x(\partial \bar{T}/\partial x)$, the meridional component $-v'_y(\partial \bar{T}/\partial y)$ plays an dominant role in both explaining temperature standard deviation and skewness. This result shows that meridional asymmetry of temperature gradient is a more significant source of temperature skewness than the zonally asymmetry, as was also mentioned in Tamarin-Brodsky et al. (2020).

In summary, the theory in Eqs. (8) and (9) suggests that temperature variance and skewness can be attributed to the symmetry and asymmetry in conditional temperature advection between anomalous warm and cold events, respectively. The symmetrical component in conditional temperature advection is mostly explained by anomalous advection of stationary temperature gradient, but the asymmetrical component is largely governed by anomalous advection of both stationary and transient temperature gradients.

5. Examining the Newtonian relaxation approximation above land

The linear relationship between conditional temperature advection and the temperature PDF has been shown to be a good first-order approximation, but we would like to go one

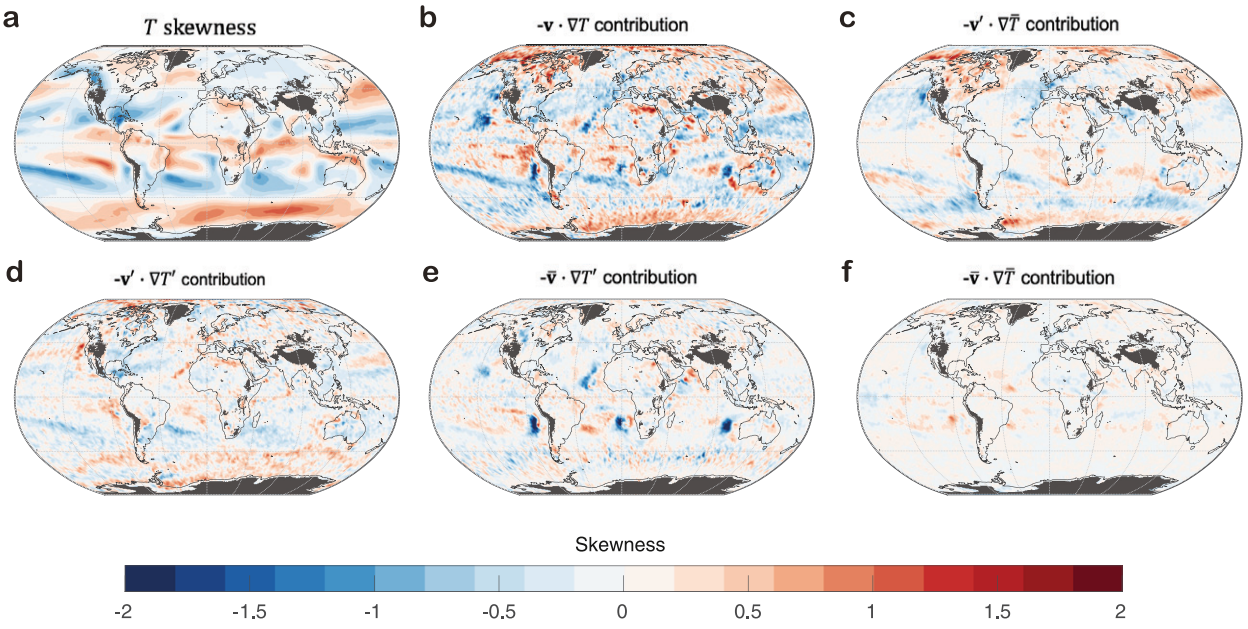

FIG. 8. As in Fig. 6, but for DJF. The pattern correlation between (a) and (b) is 0.34.

step beyond that to see how robust it is and to explore the role of other processes. Since the extremes happening on land have the most important impact on human society, we narrow down our scope to land and exclude the Antarctic. We applied the *k*-means clustering analysis algorithm (e.g., Loikith et al. 2013; Wilks 2011) on the combined vector (98-point vector) of locally normalized conditional temperature advection and locally normalized conditional average temperature at each grid point over land, and the results are shown as Fig. 9a (JJA) and Fig. 10a (DJF). Here we use the Euclidean distance function to calculate distances between clusters, and the numbers of clusters are chosen as 6 for JJA and 7 for DJF. To decide these numbers, we increased the numbers of clusters by one per iteration, beginning at 3, until there are no significant changes in the spatial patterns of the clustering maps—that is, until there are no radical rearrangements of clusters but simply splitting existing clusters into smaller ones. The *k*-means++ algorithm (e.g., Arthur and Vassilvitskii 2006) is used for cluster center initialization. We replicate the clustering process 100 times and choose the result with the smallest total sum of distance. Note that when calculating the clusters, we do not weight the grid cells by their area. When we calculate the centroids for each cluster both with and without weighting the data with the area of the grid cells, we find that the difference between them is negligible. The grid-cell-area-weighted results are shown in Fig. 9b (JJA) and Fig. 10b (DJF), and the simple averaged result is not shown here.

For JJA, as shown in Fig. 9, there are relatively consistent linear relationships between conditional advection and temperatures in clusters 1, 2, and 4, which cover more than 60% of the area, and the positive linear correlations between conditional temperature advection and percentile average temperature in these three clusters are relatively significant. For the first cluster (Fig. 9b) that linear relationship is good along all percentiles, whereas in the second and fourth clusters there are turning points beyond which the relationship no longer holds. Compositing all the points in each clusters, we can find the turning point for the second and fourth clusters is around the 50th percentile; that is, the framework in Eq. (5) explains about half of the temperature distributions with all other terms except the conditional temperature advection acting as a simple damping. The positive linear relationship is also evident for the lower half of cluster 5 (Fig. 9b); however, temperature and conditional temperature advection are anticorrelated. For the other two clusters covering about 20% of total area, the percentile temperature average does not change monotonically with conditional temperature advection, which means that the conditional temperature advection cannot explain the shape of the temperature distribution. The first-order Taylor expansion with constant coefficients [Eq. (2)] clearly is not appropriate here. The classification of the advection–temperature relationships can also serve as a useful tool to understand how temperature extremes can be related to different processes. For example, extreme heat events at a location in cluster 1 or 4 can be likely explained by horizontal temperature advection, while those events at locations in cluster 2 or 3 are more likely caused by processes other than horizontal advection.

Similar results for DJF are shown in Fig. 10, with the largest three clusters covering more than 60% of the area we are studying, where there are relatively significant positive correlations between conditional temperature advection and percentile average temperature. There are also

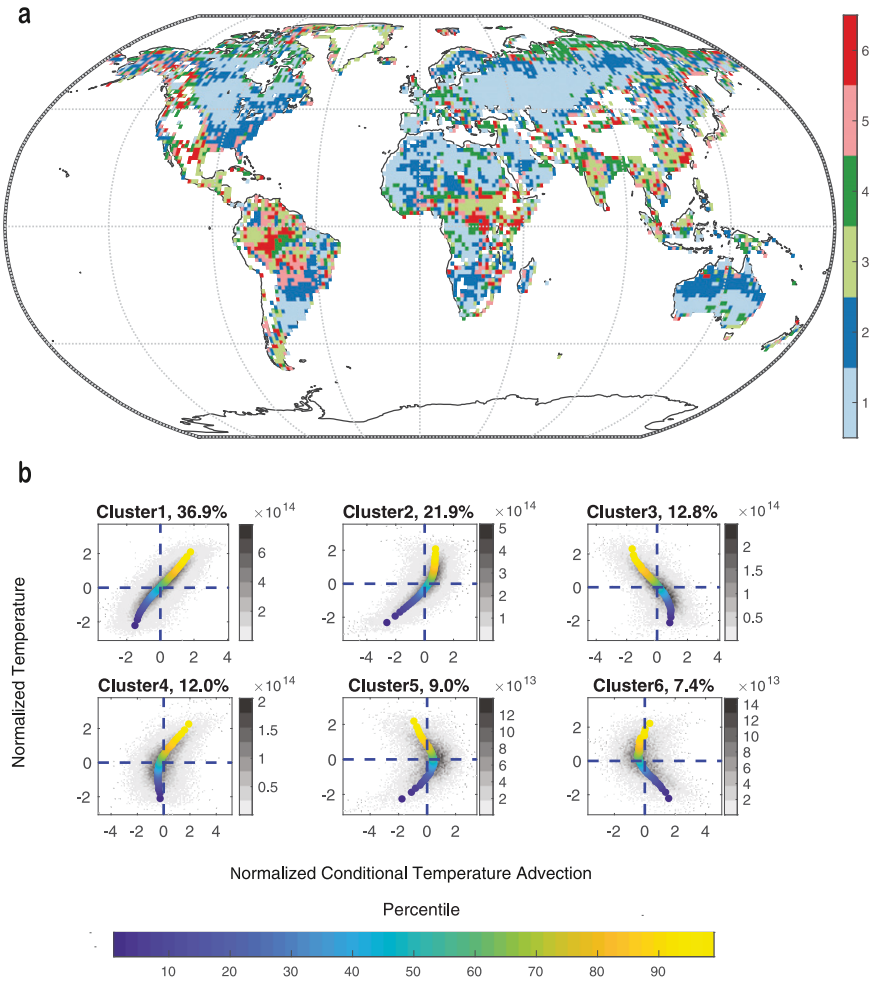

FIG. 9. A *k*-means clustering analysis of the combined vector of ERA5 850-hPa JJA temperature and conditional temperature advection data above land. (a) Spatial map of the clusters. (b) Scatterplots (black-and-white points; the shading shows the grid-cell-area-weighted density of points in m^2, as in Fig. 3) of temperature vs conditional temperature advection at all the grid points shown in Fig. 9a in the corresponding clusters, and the grid-cell-area-weighted centroids (colored points, the color shows the percentile of temperature) of all the scatterplots in each cluster. (Similar to the calculation of grid-cell-area-weighted densities for the scatterplots, when calculating the centroids, the data are weighted by the areas of the grid cells where the data come from). The labels show the relative total area coverage of each cluster.

turning points around the 50th percentile for clusters 2 and 3, which are similar to the behaviors of clusters 2 and 4 for JJA, respectively. The linear clusters are also dominant above midlatitudes. For the other four clusters, the Newtonian relaxation parameterization [Eq. (2)] also cannot properly explain the relationships between the conditional temperature advection and temperature distributions. It is interesting that we see the linear clusters (clusters 1, 2, and 3) covers larger areas in the Northern Hemisphere, and smaller areas in the Southern Hemisphere in DJF than JJA, which reflects a shift of the advection–temperature relationships with seasons. Indeed, we see the fully anticorrelated cluster (cluster 3 in JJA, and cluster 5 in DJF) also moves to the south in DJF. Considering the similarity between the features of JJA and DJF clustering results (Fig. 9 and Fig. 10, respectively), in the rest of this section we choose to examine JJA as an example to further explore the role of four different stationary and transient components of conditional mean horizontal advections, as well as the vertical transport and diabatic processes in different clusters.

To better interpret the role of the four different stationary and transient components of conditional mean horizontal temperature advection [discussed in section 4 and Eq. (7)] in shaping temperature distributions in each cluster, each of the four components is locally normalized (normalized at each

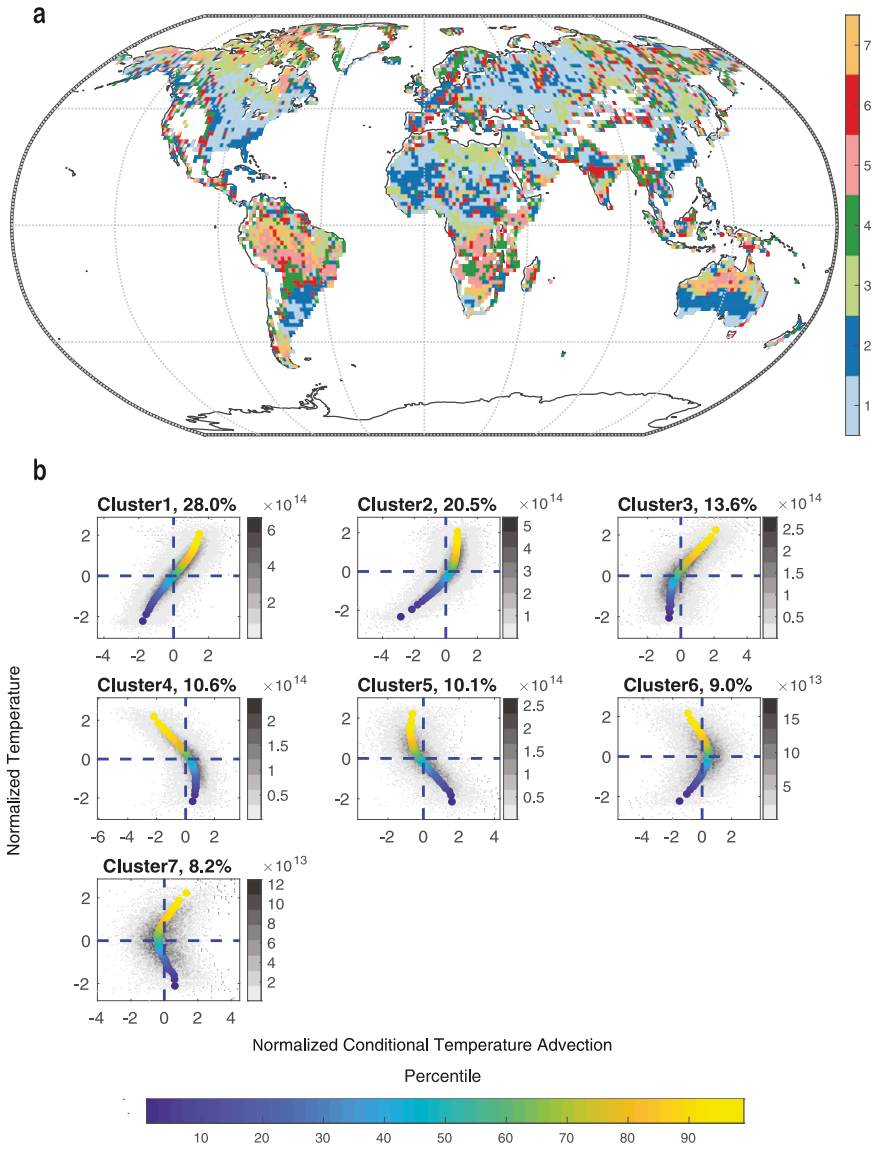

FIG. 10. As in Fig. 9, but for DJF.

grid point through first subtracting the mean of the corresponding term across the 49 conditional mean value, then divided by the standard deviation of the 49 values of conditional mean of the full horizontal temperature advection term) and averaged across all the corresponding grid points in each cluster (when doing the average, the data are weighted by the area of the grid cell where they come from) and plotted against the temperature across different percentiles in Fig. 11. Note that although we would expect the sum of the four components to be equal to the full horizontal temperature advection at each grid point, as shown in Eq. (7), this is not true in Fig. 11 due to the normalization process and averaging. Figure 11 shows that the conditional mean of anomalous advection of stationary temperature term $-\mathbf{v}' \cdot \nabla \bar{T}$ always has a positive correlation with the temperature, which is consistent with the findings of a couple of previous studies (Schneider et al. 2015; Tamarin-Brodsky et al. 2019). The stationary advection of stationary temperature gradient term $-\bar{\mathbf{v}} \cdot \nabla \bar{T}$ across different temperature percentiles is always small. However, the role of the full conditional temperature advection is complicated by the other two components, that is, the covariance between the anomalous wind and anomalous temperature gradient $-\mathbf{v}' \cdot \nabla T'$ and the stationary advection of anomalous temperature gradient $-\mathbf{v}' \cdot \nabla T'$, whose relationships with the temperature are different in different clusters.

To allow a somewhat deeper understanding of the behavior of different components of advection, composites of winds and temperatures are shown in Fig. 12a, for two

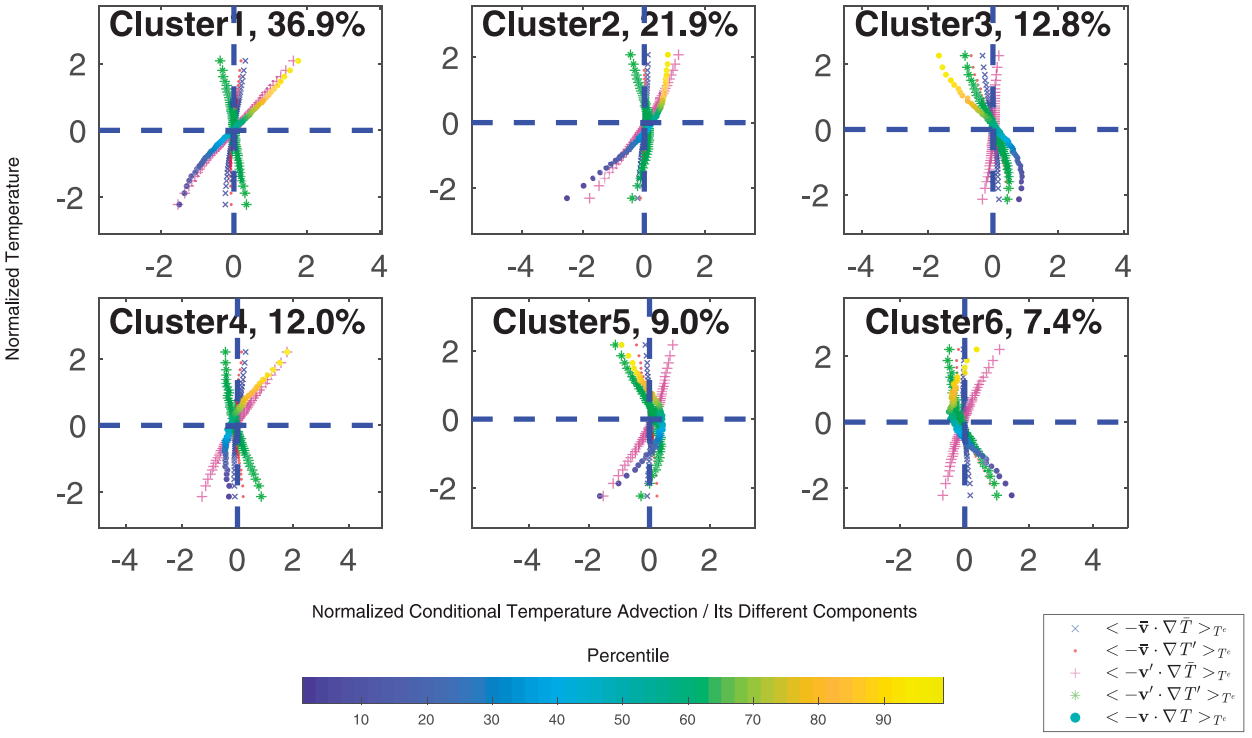

FIG. 11. The relationships between normalized percentile mean temperature T^e in JJA and normalized conditional mean of four stationary and transient components of horizontal temperature advection $\langle -\bar{\mathbf{v}}\cdot\nabla\bar{T}\rangle_{T^e}$, $\langle -\bar{\mathbf{v}}\cdot\nabla T'\rangle_{T^e}$, $\langle -\mathbf{v}'\cdot\nabla\bar{T}\rangle_{T^e}$, and $\langle -\mathbf{v}'\cdot\nabla T'\rangle_{T^e}$ (normalized at each location by subtracting the mean of each term across all percentiles, and then divided by the standard deviation of the full conditional horizontal temperature advection term across all percentiles) averaged with area-weighting in each cluster shown in Fig. 9. The area-weighted centroids shown in Fig. 9 are plotted here again as a reference in the colored points, with percentile indicated by the color.

different locations (33°N, 88°W and 24°S, 120°E) chosen in cluster 2 of Fig. 9. The relationships between temperature and conditional temperature advection (and its four different components) are shown in Fig. 12b, and we can confirm that the behaviors of conditional temperature advection at these chosen locations are qualitatively consistent with the cluster two of Fig. 9. For the location in the southeast United States (33°N, 88°W), at lower percentiles (5th–10th) of temperature we can observe a very weak positive advection $\langle -\mathbf{v}\cdot\nabla T\rangle_{T^e}$. Although the normalized result in Fig. 12b shows a negative result, it does not necessarily mean that the actual value is positive. The advection $\langle -\mathbf{v}\cdot\nabla T\rangle_{T^e}$ keeps increasing from a temperature percentile range of 5%–10% to a temperature percentile range of 47.5%–52.5%, and then to 90%–95%, but it can be observed from Fig. 12b that the full advection increases far more at the lower half of temperature distribution than the upper half. Similarly, the anomalous advection of stationary temperature gradient $\langle -\mathbf{v}'\cdot\nabla\bar{T}\rangle_{T^e}$ increases from a negative value to a positive value from a temperature percentile range of 5%–10% to 47.5%–52.5%, but does not increase much from 47.5%–52.5% to 90%–95%. The behavior of the anomalous advection of anomalous temperature gradient $\langle -\mathbf{v}'\cdot\nabla T'\rangle_{T^e}$ term is slightly different from the centroid we get in Fig. 11 and here it keeps increasing from the lower percentile to the upper percentile. For the stationary advection of the anomalous temperature gradient $\langle -\bar{\mathbf{v}}\cdot\nabla T'\rangle_{T^e}$, we see that the wind at the chosen location is always in similar directions to the contour, and thus $\langle -\bar{\mathbf{v}}\cdot\nabla T'\rangle_{T^e}$ is always small. The stationary advection of stationary temperature gradient $\langle -\bar{\mathbf{v}}\cdot\nabla\bar{T}\rangle_{T^e}$ is not presented here, but it does not change much with percentile and thus has small contribution to the temperature distribution. For the location in east Australia (24°S, 120°E), the behavior of different components of advection in Fig. 12b are more similar to the centroid of cluster 2 in Fig. 9. The behaviors of the full advection term $\langle -\mathbf{v}\cdot\nabla T\rangle_{T^e}$ and the anomalous advection of stationary temperature gradient $\langle -\mathbf{v}'\cdot\nabla\bar{T}\rangle_{T^e}$ are quite similar: both of them increase from a temperature percentile range of 5%–10% to 47.5%–52.5%, and then to 90%–95%, and increase faster at the lower part than the upper part of the temperature PDFs. The anomalous advection of anomalous temperature gradient $\langle -\mathbf{v}'\cdot\nabla T'\rangle_{T^e}$ is small for the lower percentiles of temperature (5th–10th), due to the relatively small temperature gradient of the anomalous temperature at this location. At middle percentiles of temperature (47.5%–52.5%), $\langle -\mathbf{v}'\cdot\nabla\bar{T}\rangle_{T^e}$ is quite small, and at high percentiles it brings cold advection again, to the temperature maximum; thus, the $\langle -\mathbf{v}'\cdot\nabla T'\rangle_{T^e}$ gives lower values at

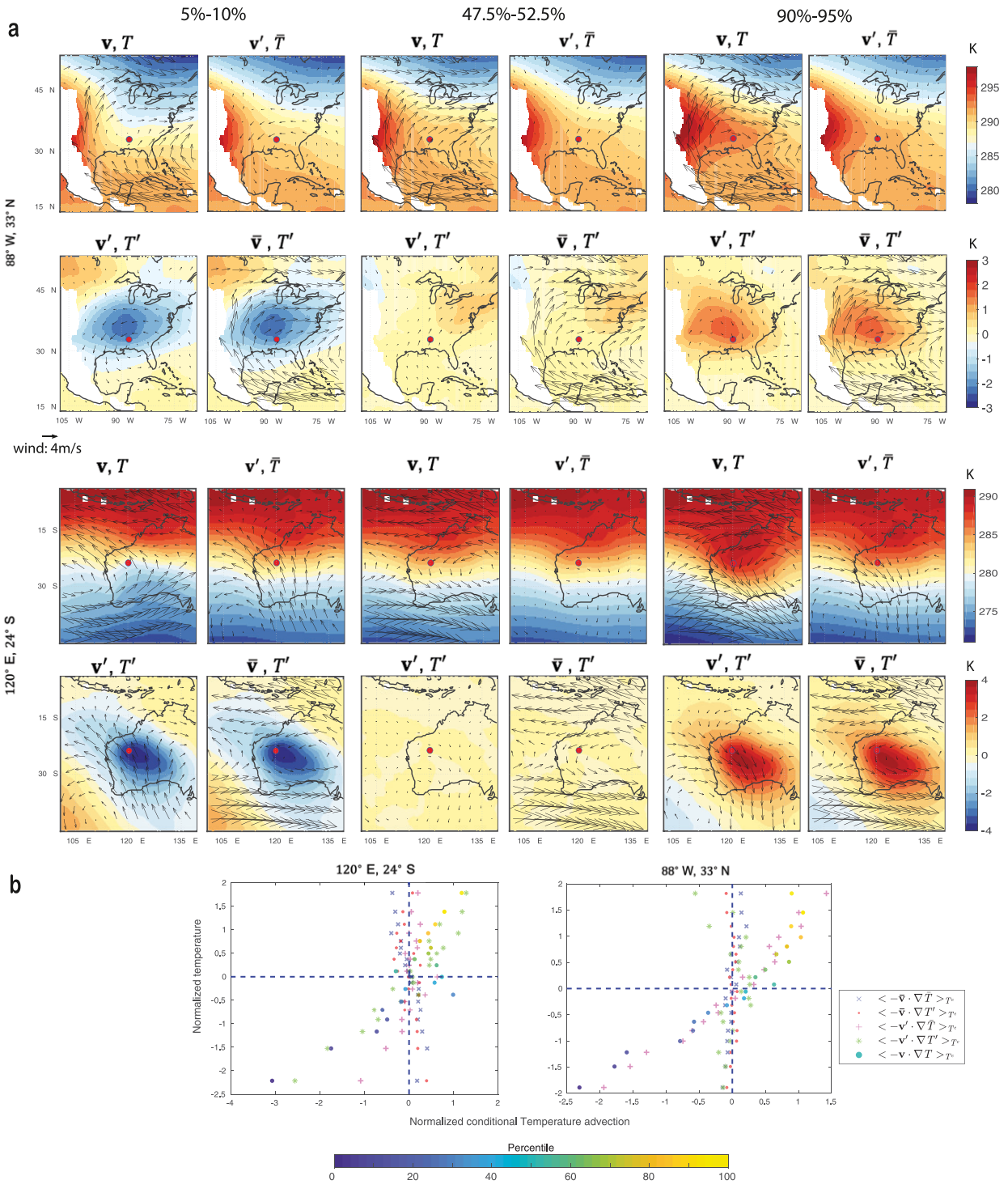

FIG. 12. (a) A composite of 850-hPa JJA stationary and transient winds in vectors and temperature [($\mathbf{v}$, T), ($\mathbf{v}'$, $\bar{T}$), ($\mathbf{v}'$, T'), ($\bar{\mathbf{v}}$, T')] in contours around the locations indicated by the red dots, for temperature at percentile ranges of [5%–10%], [47.5%–52.5%], and [90%–95%], respectively. Two locations (33°N, 88°W and 24°S, 120°E) from cluster 2 in Fig. 9 are chosen. (b) Scatterplots for the normalized conditional temperature advection and normalized temperature at these locations. Here only 19 percentile bins ([2.5%–7.5%], [7.5%–12.5%], …, [92.5%–97.5%]), instead of 49, are used to reduce noise. The color bar shows the percentiles for the full conditional temperature advection terms $\langle -\mathbf{v}\cdot\nabla T\rangle_{T^c}$. The temperature, wind, and advection calculated from the original data are smoothed to 1.5° × 1.5° resolution when calculating the composites.

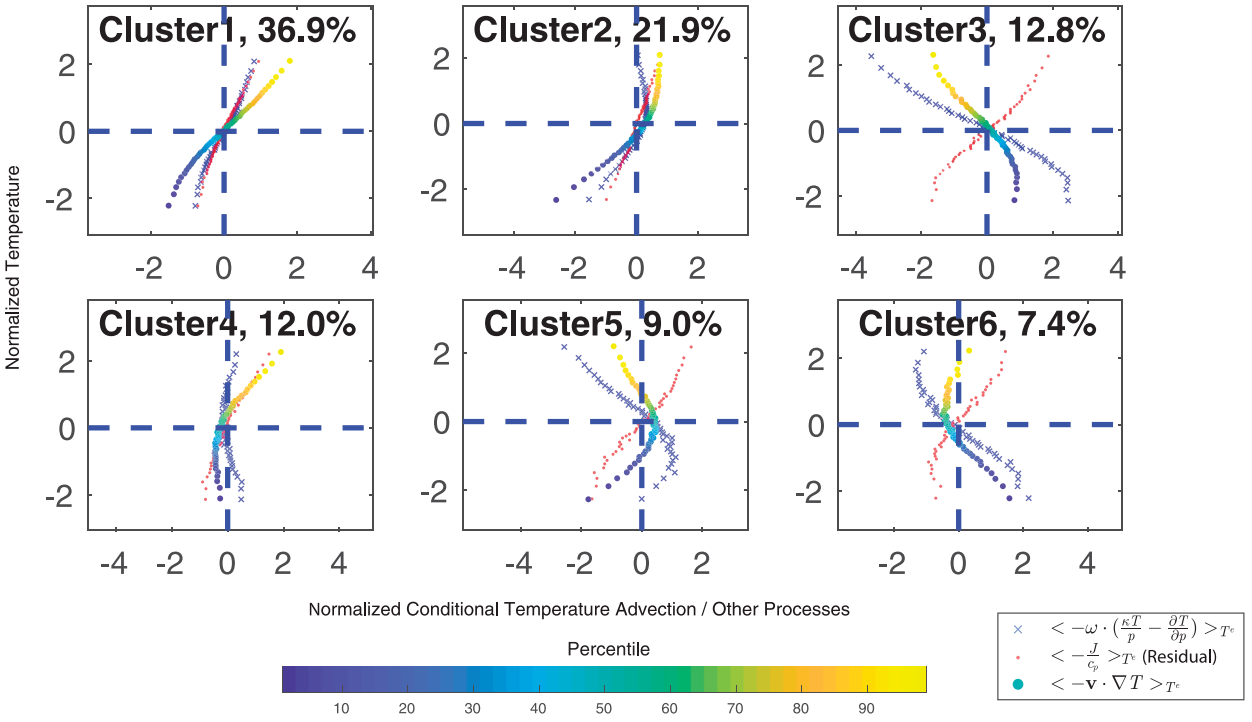

FIG. 13. The relationships between normalized percentile mean temperature T^e in JJA and normalized negative conditional mean vertical processes and normalized negative conditional mean diabatic processes (normalized at each location by subtracting the mean of each term across all percentiles, and then divided by the standard deviation of the full horizontal temperature advection term across all percentiles) averaged with area-weighting in each cluster shown in Fig. 9. The grid-cell-area-weighted centroids are as in Fig. 11.

both end of temperature distributions. Again, the $\langle -\bar{\mathbf{v}} \cdot \nabla T' \rangle_{T^e}$ term is still small and the $\langle -\bar{\mathbf{v}} \cdot \nabla \bar{T} \rangle_{T^e}$ term does not change much with percentile, so they have small contributions to the temperature distribution. These two points are in very different regions, but based on this clustering analysis they should have similar behaviors, and overall these composites suggest that is indeed the case.

We next investigate the role of the other processes parameterized by the Newtonian relaxation [the first-order Taylor expansion in Eq. (2)]. Expanding the $\dot{T}$ term in Eq. (1) using the first law of thermodynamics, we have

$$\frac{\partial T}{\partial t} = -\mathbf{v} \cdot \nabla T - \omega \frac{\partial T}{\partial p} + \omega \frac{\kappa T}{p} + \frac{J}{c_p}, \tag{10}$$

where $\kappa = R_d/c_p$ and J are the diabatic heating processes, such as latent heat release, radiation, and heat fluxes from the boundary layer. The comparison of Eqs. (10) and (3) shows that the processes we have treated as a Newtonian relaxation are the combination of the vertical advection, adiabatic expansion, and diabatic processes [$\omega(\kappa T/p)$, $-\omega(\partial T/\partial p)$, and J/c_p, respectively]. Applying the conditional mean framework to Eq. (10), we have

$$\left\langle \frac{\partial T}{\partial t} \right\rangle_{T^e} = \langle -\mathbf{v} \cdot \nabla T \rangle_{T^e} + \left\langle \omega \left(\frac{\kappa T}{p} - \frac{\partial T}{\partial p} \right) \right\rangle_{T^e} + \left\langle \frac{J}{c_p} \right\rangle_{T^e}. \tag{11}$$

Because $\langle \partial T/\partial t \rangle_{T^e} \approx 0$ as has been discussed in section 2a, and also taking Eq. (4) into account, Eq. (11) can be written as

$$\langle -\mathbf{v} \cdot \nabla T \rangle_{T^e} = -\left(-\frac{\langle T \rangle_{T^e} - T_{\text{eq}}}{\tau} \right) = -\left\langle \omega \left(\frac{\kappa T}{p} - \frac{\partial T}{\partial p} \right) \right\rangle_{T^e} - \left\langle \frac{J}{c_p} \right\rangle_{T^e}. \tag{12}$$

That is, the conditional temperature advection equals the negative of the conditional mean of the processes described by the Newtonian relaxation (first-order Taylor expansion) in Eq. (2), which is actually a combination of the negative of the conditional mean of the combined vertical transport term $-\langle \omega(\kappa T/p - \partial T/\partial p) \rangle_{T^e}$ and the negative of the conditional mean of the diabatic process $-\langle J/c_p \rangle_{T^e}$. Thus examining how these processes change with the percentile mean of temperature T^e can improve our understanding of how well they can be described with the Newtonian relaxation, and how well the temperature T^e can be linearly explained by conditional temperature advection $\langle -\mathbf{v} \cdot \nabla T \rangle_{T^e}$.

Similar to Fig. 11, Fig. 13 shows the locally normalized negative conditional mean vertical transport process $-\langle \omega(\kappa T/p - \partial T/\partial p) \rangle_{T^e}$ and negative conditional mean diabatic process $-\langle J/c_p \rangle_{T^e}$ averaged across all the grid points in each cluster (when doing the average, the data are also weighted by the area of the grid cell where they come from, similar to what we do for Fig. 11). Here $\omega(\kappa T/p - \partial T/\partial p)$ and J/c_p are normalized respectively at each grid point through first subtracting the mean of the corresponding term across the 49 conditional mean value, then divided by the standard deviation of the 49 values of conditional mean of the full

horizontal temperature advection term. This normalization by the standard deviation of the conditional temperature advection enables comparison of relative magnitudes of these different terms. When calculating $-\langle\omega(\kappa T/p-\partial T/\partial p)\rangle_{T^e}$ and $-\langle J/c_p\rangle_{T^e}$ at each grid point, the $-\langle\omega(\kappa T/p-\partial T/\partial p)\rangle_{T^e}$ term is directly calculated from the ERA5 data, and $-\langle J/c_p\rangle_{T^e}$ at each grid point is calculated as the difference of $\langle-\mathbf{v}\cdot\nabla T\rangle_{T^e}$ and $-\langle\omega(\kappa T/p-\partial T/\partial p)\rangle_{T^e}$, as described in Eq. (12). From Fig. 13, it can be observed that the negative conditional mean of the vertical transportation process $-\langle\omega(\kappa T/p-\partial T/\partial p)\rangle_{T^e}$ has similar magnitude of changes with the change of temperature T^e as the negative conditional mean of the diabatic term $-\langle J/c_p\rangle_{T^e}$. Note that $-\langle J/c_p\rangle_{T^e}$ has positive and relatively linear relationships with T^e in all the clusters, while the relationship between $-\langle\omega(\kappa T/p-\partial T/\partial p)\rangle_{T^e}$ and T^e is only relatively good in the first. Thus we can come to the conclusion that comparing to the diabatic processes J/c_p, the vertical transport process $\omega(\kappa T/p-\partial T/\partial p)$ plays a more complex role in both driving the $\dot{T}$ term in Eq. (1) away from the Newtonian relaxation in Eq. (2), and explaining the nonlinearity of the relationship between conditional temperature advection $\langle-\mathbf{v}\cdot\nabla T\rangle_{T^e}$ and percentile mean temperature T^e. A visualization on the change of vertical transport $\langle\omega(\kappa T/p-\partial T/\partial p)\rangle_{T^e}$ with percentiles of temperature in JJA is shown in Fig. S3. We can see that the vertical transport $\langle\omega(\kappa T/p-\partial T/\partial p)\rangle_{T^e}$ indeed decreases with the percentile of temperature above a large portion of the grid points, which means it works more like a relaxation force, driving the temperature anomalies back to the equilibrium temperatures. However, exceptions can also be found, such as in the deep tropics and over India, where the vertical transport is positively correlated with the temperature. These are also where the conditional temperature advection is not positively correlated with temperature (clusters 3, 5, and 6), and we hypothesize that significant negative correlations may be related to the anticorrelation of conditional mean vertical transport of temperature with the horizontal divergence of the winds in a region with a small temperature gradient.

6. Discussion and conclusions

In this paper, we have studied the balance between atmospheric temperature advection and other physical processes in shaping daily temperature PDFs based on the conditional mean framework developed in Linz et al. (2020). Linz et al. (2020) analyzed the physics setting the temperature PDF in idealized aquaplanet simulations and found that in midlatitudes the majority of the shape of the PDF can be explained by the conditional mean of horizontal advection, with the linear parameterization of the other processes constant across percentiles. Our current study applies that framework to ERA5 data for both JJA and DJF seasons, and we find the relationship claimed above in Linz et al. (2020) still largely holds true. The linear correlation between conditional temperature advection and percentile mean of temperature itself is relatively high, especially above midlatitude oceans in the Southern Hemisphere. The horizontal temperature advection does not explain the shape of the temperature distribution near orography, and this is consistent with the important role of topography in affecting the nearby variance through changes in the local thermal structure (e.g., Lutsko et al. 2019). Some of the disagreement may also be due to the choice of looking at 850 hPa rather than the surface, and while this framework could be useful for examining temperature distributions near orography, we do not do so here. In the deep tropics where the role of advection is expected to be small, we see that horizontal temperature advection does not explain the shape of temperature distribution.

The conditional mean framework has been further applied to different components of the conditional temperature advection to explore the role of different transient and stationary terms in influencing temperature variance and skewness. Consistent with previous studies (Garfinkel and Harnik 2017; Schneider et al. 2015; Tamarin-Brodsky et al. 2019), we find that the major term related to the variance of the temperature PDF is the anomalous advection of the stationary temperature gradient $-\mathbf{v}'\cdot\nabla\bar{T}$, thus supporting the mixing length theory explaining the dynamical origin of temperature variance proposed in Schneider et al. (2015) and Tamarin-Brodsky et al. (2019). On the other hand, we find that both the anomalous advection of stationary temperature gradient $-\mathbf{v}'\cdot\nabla\bar{T}$ and the covariance between anomalous wind and anomalous temperature $-\mathbf{v}'\cdot\nabla T'$ play an important role for temperature skewness. This is an interesting result and is consistent with Tamarin-Brodsky et al.'s (2020) recent result for Northern Hemisphere; although it is commonly agreed that $-\mathbf{v}'\cdot\nabla T'$ is important for temperature skewness (Garfinkel and Harnik 2017; Linz et al. 2018; Tamarin-Brodsky et al. 2019) with symmetric temperature gradients, we show that the contribution of the $-\mathbf{v}'\cdot\nabla\bar{T}$ term is even more important in the real world.

To understand in more detail where the linear relationship between conditional temperature advection and temperature holds true above land, we tested the robustness of the assumption of treating all the physical processes other than horizontal advection as a Newtonian relaxation by identifying regions with qualitatively different advection–temperature relationships using k-means clustering analysis in both JJA and DJF. We find that for JJA 37% of the land area can be well explained by the first-order Taylor expansion (cluster 1), and this land is primarily in the midlatitudes, including most of eastern Europe and the eastern half of the United States. For about another 30% of the land area (clusters 2 and 4), such an approximation can readily explain either the lower half or the upper half of the temperature PDF. These clusters have less spatial coherence than the first cluster, but the second cluster tends to be mostly at the edge of the tropics, which is especially evident in the Southern Hemisphere. The first and fourth clusters are dominant in western Europe, suggesting that the shape of the temperature distribution at the upper extreme end in there is well explained by the horizontal temperature advection. It is interesting to note that Bieli et al. (2015)

and Zschenderlein et al. (2019) studied several different regions and argue that the horizontal temperature advection is not the primary mechanism causing heat waves. We find the regions that Zschenderlein et al. (2019) studied fall into different clusters. Western Russia, the Iberian Peninsula, and the British Isles fall mainly into clusters 1 and 4 where temperature advection does explain the upper part of the distribution, and this is inconsistent with their results. Scandinavia and southern Italy fall into clusters 2, 5, and 6, consistent with their results. The approaches in these studies differ, and it is clear that regional heatwaves need further study. For DJF, the first-order Taylor expansion also works well in the largest cluster, which covers about 30% of the total area; in the following two clusters, covering another 30% of the total area, either the lower half or the upper half of the temperature PDF can be well explained. The linear clusters are still dominant above the midlatitudes, and we can see a shift of the linear clusters with season to the south from JJA to DJF.

Considering the similarity between JJA and DJF, we choose to take JJA as an example to explore the role of different stationary components, as well as the role of vertical transportation and diabatic processes in shaping temperature PDFs. We find that except for cluster 1, the role of other physical processes—that is, vertical transport $\omega(\kappa T/p - \partial T/\partial p)$ and diabatic processes J/c_p—cannot be sufficiently represented with the first-order Taylor expansion with constant coefficients that we have expressed here as a Newtonian relaxation. Our analysis shows that the vertical transport $\omega(\kappa T/p - \partial T/\partial p)$ (vertical advection and adiabatic expansion) plays a more complex role in driving the relationship between conditional temperature advection $\langle -\mathbf{v}\cdot\nabla T\rangle_{T^e}$ and percentile mean temperature T^e away from linear. The diabatic process J/c_p, however, has a relatively more linear relationship with temperature under the conditional mean framework and a smaller influence on the robustness of the first-order Newtonian relaxation approximation. We also examine the relationships of different stationary and transient components of horizontal temperature advection $\langle -\mathbf{v}\cdot\nabla T\rangle_{T^e}$ with percentile mean temperature T^e in the different clusters and find that the conditional mean of anomalous advection of stationary temperature gradient $\langle -\mathbf{v}'\cdot\nabla\bar{T}\rangle_{T^e}$ has a positive correlation with the temperature T^e and the conditional mean stationary advection of stationary temperature gradient term $\langle -\bar{\mathbf{v}}\cdot\nabla\bar{T}\rangle_{T^e}$ across different temperature percentiles is small. The other two components, the conditional mean of anomalous wind and anomalous temperature gradient $\langle -\mathbf{v}'\cdot\nabla T'\rangle_{T^e}$ and the conditional mean of the stationary advection of anomalous temperature gradient $\langle -\bar{\mathbf{v}}\cdot\nabla T'\rangle_{T^e}$, have more complex relationships with the temperature T^e, which differ from cluster to cluster.

We caution that none of the relationships we have identified here are obviously causal. We have not evaluated lead–lag relationships or the specifics of the meteorology of composites for the tails. This method, while informative, is descriptive and needs to be considered in combination with other approaches to understanding temperature distributions. Untangling the roles of different physical processes in shaping temperature distributions will help to predict how they will change with climate change. Although the conditional mean framework of Linz et al. (2020) is suitable to answer them, we have not addressed the following two important questions in the current study: How will climate change regulate the advection–temperature relationship? And how will the temperature PDF change with the changes of all the different physical controlling processes? We only focused on a single climate state in this study, but the analysis can be applied to study the change of advection and temperature PDFs between climate states (e.g., using comprehensive climate model output), and this is the topic of ongoing work.

Acknowledgments. We thank two anonymous reviewers and Chaim Garfinkel for providing excellent, constructive reviews. We thank Todd Mooring, Da Nian, and Kevin Stephen for helpful discussions. GC and ML acknowledge support from NSF awards AGS-1742178 and AGS-1608775. The ERA5 data were downloaded using Copernicus Climate Change Service information (2020).

Data availability statement. The ERA5 hourly data on pressure levels from 1979 to present dataset used in this study can be accessed through Copernicus Climate Change Service (C3S) at https://doi.org/10.24381/cds.bd0915c6.

APPENDIX

Derivation of the Approximate Contribution of Horizontal Temperature Advection to Temperature Variance and Skewness

Consider horizontal temperature advection, $-\mathbf{v}\cdot\nabla T$: define $(-\mathbf{v}\cdot\nabla T)_{w0}$ as the warmer part, (i.e., the mean value of temperature advection on the condition that temperature T is larger than its mean value) and define $(-\mathbf{v}\cdot\nabla T)_{c0}$ as the colder part (i.e., the mean value of temperature advection on the condition that temperature T is smaller than its mean value). Also define $(-\mathbf{v}\cdot\nabla T)_{\bar{T}}$ as the value of horizontal temperature advection on the condition that the temperature is at its mean value. Using Eq. (5), the contribution of advection to the warmer part of temperature PDF, T_{w0} (i.e., the mean value of temperature on that condition that T is larger than $\bar{T}$) and the colder part of temperature PDF T_{c0} (i.e., the mean value of temperature on that condition that T is smaller than $\bar{T}$) could be expressed as

$$T_{w0} - \bar{T} = \tau \times \left[(-\mathbf{v}\cdot\nabla T)_{w0} - (-\mathbf{v}\cdot\nabla T)_{\bar{T}}\right] \tag{A1}$$

and

$$T_{c0} - \bar{T} = \tau \times \left[(-\mathbf{v}\cdot\nabla T)_{w0} - (-\mathbf{v}\cdot\nabla T)_{\bar{T}}\right], \tag{A2}$$

respectively. If we define

$$T_w = T_{w0} - \bar{T} \text{ and } T_c = \bar{T} - T_{c0}, \tag{A3}$$

$$(-\mathbf{v}\cdot\nabla T)_w = (-\mathbf{v}\cdot\nabla T)_{w0} - (-\mathbf{v}\cdot\nabla T)_{\bar{T}}, \tag{A4}$$

$$(-\mathbf{v}\cdot\nabla T)_c = (-\mathbf{v}\cdot\nabla T)_{\bar{T}} - (-\mathbf{v}\cdot\nabla T)_{c0}, \tag{A5}$$

according to Eqs. (1) and (2) in Tamarin-Brodsky et al. (2020), we have

$$\sigma^2_{-\mathbf{v}\cdot\nabla T} = \left[\frac{1}{2}\times(T_w + T_c)\right]^2 = \left\{\frac{1}{2}\times\tau\times\left[(-\mathbf{v}\cdot\nabla T)_w + (-\mathbf{v}\cdot\nabla T)_c\right]\right\}^2 \tag{A6}$$

and

$$S_{-\mathbf{v}\cdot\nabla T} = \frac{T_w - T_c}{\frac{1}{2}\times(T_w + T_c)} = \frac{\tau\times\left[(-\mathbf{v}\cdot\nabla T)_w - (-\mathbf{v}\cdot\nabla T)_c\right]}{\sigma_T}. \tag{A7}$$

Here, τ is the relaxation time scale, and σ_T is the real standard deviation of temperature time series. Note that our interpretation for T_w and T_c is slightly different from the original meaning in Tamarin-Brodsky et al. (2020), although the validity of Eqs. (A6) and (A7) should remain the same. In Tamarin-Brodsky et al. (2020), the definition of T_w and T_c are the average absolute intensities of warm and cold anomalies identified by their Lagrangian feature tracking algorithm, and are always positive, whereas our $(-\mathbf{v}\cdot\nabla T)_w$ and $(-\mathbf{v}\cdot\nabla T)_c$ here could have negative values where the correlations between conditional advection and temperature are low.

REFERENCES

Alexander, L., and S. Perkins, 2013: Debate heating up over changes in climate variability. *Environ. Res. Lett.*, **8**, 041001, https://doi.org/10.1088/1748-9326/8/4/041001.

Arthur, D., and S. Vassilvitskii, 2006: k-means++: The advantages of careful seeding. Tech. Rep. 2006-13, Stanford InfoLab, 9 pp.

Barnes, E. A., and J. A. Screen, 2015: The impact of Arctic warming on the midlatitude jet-stream: Can it? Has it? Will it? *Wiley Interdiscip. Rev.: Climate Change*, **6**, 277–286, https://doi.org/10.1002/wcc.337.

Bieli, M., S. Pfahl, and H. Wernli, 2015: A Lagrangian investigation of hot and cold temperature extremes in Europe. *Quart. J. Roy. Meteor. Soc.*, **141**, 98–108, https://doi.org/10.1002/qj.2339.

Buzan, J. R., and M. Huber, 2020: Moist heat stress on a hotter Earth. *Annu. Rev. Earth Planet. Sci.*, **48**, 623–655, https://doi.org/10.1146/annurev-earth-053018-060100.

Cade, B. S., and B. R. Noon, 2003: A gentle introduction to quantile regression for ecologists. *Front. Ecol. Environ.*, **1**, 412–420, https://doi.org/10.1890/1540-9295(2003)001[0412:AGITQR]2.0.CO;2.

Chen, G., J. Norris, J. D. Neelin, J. Lu, L. R. Leung, and K. Sakaguchi, 2019: Thermodynamic and dynamic mechanisms for hydrological cycle intensification over the full probability distribution of precipitation events. *J. Atmos. Sci.*, **76**, 497–516, https://doi.org/10.1175/JAS-D-18-0067.1.

Coumou, D., J. Lehmann, and J. Beckmann, 2015: The weakening summer circulation in the Northern Hemisphere midlatitudes. *Science*, **348**, 324–327, https://doi.org/10.1126/science.1261768.

——, G. Di Capua, S. Vavrus, L. Wang, and S. Wang, 2018: The influence of Arctic amplification on mid-latitude summer circulation. *Nat. Commun.*, **9**, 2959, https://doi.org/10.1038/s41467-018-05256-8.

Gao, Y., L. R. Leung, J. Lu, and G. Masato, 2015: Persistent cold air outbreaks over North America in a warming climate. *Environ. Res. Lett.*, **10**, 044001, https://doi.org/10.1088/1748-9326/10/4/044001.

Garfinkel, C. I., and N. Harnik, 2017: The non-Gaussianity and spatial asymmetry of temperature extremes relative to the storm track: The role of horizontal advection. *J. Climate*, **30**, 445–464, https://doi.org/10.1175/JCLI-D-15-0806.1.

Grotjahn, R., and Coauthors, 2015: North American extreme temperature events and related large scale meteorological patterns: A review of statistical methods, dynamics, modeling, and trends. *Climate Dyn.*, **46**, 1151–1184, https://doi.org/10.1007/s00382-015-2638-6.

Hersbach, H., and Coauthors, 2020: The ERA5 global reanalysis. *Quart. J. Roy. Meteor. Soc.*, **146**, 1999–2049, https://doi.org/10.1002/qj.3803.

Horton, R. M., J. S. Mankin, C. Lesk, E. Coffel, and C. Raymond, 2016: A review of recent advances in research on extreme heat events. *Curr. Climate Change Rep.*, **2**, 242–259, https://doi.org/10.1007/s40641-016-0042-x.

Hoskins, B., and T. Woollings, 2015: Persistent extratropical regimes and climate extremes. *Curr. Climate Change Rep.*, **1**, 115–124, https://doi.org/10.1007/s40641-015-0020-8.

Huybers, P., K. A. McKinnon, A. Rhines, and M. Tingley, 2014: U.S. daily temperatures: The meaning of extremes in the context of nonnormality. *J. Climate*, **27**, 7368–7384, https://doi.org/10.1175/JCLI-D-14-00216.1.

Koenker, R., and G. Bassett, 1978: Regression quantiles. *Econometrica*, **46**, 33–50, https://doi.org/10.2307/1913643.

Linz, M., G. Chen, and Z. Hu, 2018: Large-scale atmospheric control on non-Gaussian tails of midlatitude temperature distributions. *Geophys. Res. Lett.*, **45**, 9141–9149, https://doi.org/10.1029/2018GL079324.

——, ——, B. Zhang, and P. Zhang, 2020: A framework for understanding how dynamics shape temperature distributions. *Geophys. Res. Lett.*, **47**, e2019GL085684, https://doi.org/10.1029/2019GL085684.

Loikith, P. C., and J. D. Neelin, 2015: Short-tailed temperature distributions over North America and implications for future changes in extremes. *Geophys. Res. Lett.*, **42**, 8577–8585, https://doi.org/10.1002/2015GL065602.

——, and ——, 2019: Non-Gaussian cold-side temperature distribution tails and associated synoptic meteorology. *J. Climate*, **32**, 8399–8414, https://doi.org/10.1175/JCLI-D-19-0344.1.

——, B. R. Lintner, J. Kim, H. Lee, J. D. Neelin, and D. E. Waliser, 2013: Classifying reanalysis surface temperature probability density functions (PDFs) over North America with cluster analysis. *Geophys. Res. Lett.*, **40**, 3710–3714, https://doi.org/10.1002/grl.50688.

Lutsko, N. J., J. W. Baldwin, and T. W. Cronin, 2019: The impact of large-scale orography on Northern Hemisphere winter synoptic temperature variability. *J. Climate*, **32**, 5799–5814, https://doi.org/10.1175/JCLI-D-19-0129.1.

Ma, W., J. Norris, and G. Chen, 2020: Projected changes to extreme precipitation along North American west coast from the CESM large ensemble. *Geophys. Res. Lett.*, **47**, e2019GL086038, https://doi.org/10.1029/2019GL086038.

McKinnon, K. A., A. Rhines, M. P. Tingley, and P. Huybers, 2016: The changing shape of Northern Hemisphere summer

temperature distributions. *J. Geophys. Res. Atmos.*, **121**, 8849–8868, https://doi.org/10.1002/2016JD025292.

Nakamura, N., and C. S. Y. Huang, 2018: Atmospheric blocking as a traffic jam in the jet stream. *Science*, **361**, 42–47, https://doi.org/10.1126/science.aat0721.

Norris, J., G. Chen, and J. D. Neelin, 2019a: Changes in frequency of large precipitation accumulations over land in a warming climate from the CESM large ensemble: The roles of moisture, circulation, and duration. *J. Climate*, **32**, 5397–5416, https://doi.org/10.1175/JCLI-D-18-0600.1.

——, ——, and ——, 2019b: Thermodynamic versus dynamic controls on extreme precipitation in a warming climate from the Community Earth System Model large ensemble. *J. Climate*, **32**, 1025–1045, https://doi.org/10.1175/JCLI-D-18-0302.1.

Perkins, S. E., 2015: A review on the scientific understanding of heatwaves—Their measurement, driving mechanisms, and changes at the global scale. *Atmos. Res.*, **164–165**, 242–267, https://doi.org/10.1016/j.atmosres.2015.05.014.

Petoukhov, V., S. Rahmstorf, S. Petri, and H. J. Schellnhuber, 2013: Quasiresonant amplification of planetary waves and recent Northern Hemisphere weather extremes. *Proc. Natl. Acad. Sci. USA*, **110**, 5336–5341, https://doi.org/10.1073/pnas.1222000110.

Quinting, J. F., and M. J. Reeder, 2017: Southeastern Australian heat waves from a trajectory viewpoint. *Mon. Wea. Rev.*, **145**, 4109–4125, https://doi.org/10.1175/MWR-D-17-0165.1.

Rhines, A., and P. Huybers, 2013: Frequent summer temperature extremes reflect changes in the mean, not the variance. *Proc. Natl. Acad. Sci. USA*, **110**, E546, https://doi.org/10.1073/pnas.1218748110.

——, K. A. McKinnon, M. P. Tingley, and P. Huybers, 2017: Seasonally resolved distributional trends of North American temperatures show contraction of winter variability. *J. Climate*, **30**, 1139–1157, https://doi.org/10.1175/JCLI-D-16-0363.1.

Ruff, T. W., and J. D. Neelin, 2012: Long tails in regional surface temperature probability distributions with implications for extremes under global warming. *Geophys. Res. Lett.*, **39**, L04704, https://doi.org/10.1029/2011GL050610.

Schneider, T., T. Bischoff, and H. Płotka, 2015: Physics of changes in synoptic midlatitude temperature variability. *J. Climate*, **28**, 2312–2331, https://doi.org/10.1175/JCLI-D-14-00632.1.

Screen, J. A., 2014: Arctic amplification decreases temperature variance in northern mid- to high-latitudes. *Nat. Climate Change*, **4**, 577–582, https://doi.org/10.1038/nclimate2268.

Seneviratne, S. I., T. Corti, E. L. Davin, M. Hirschi, E. B. Jaeger, I. Lehner, B. Orlowsky, and A. J. Teuling, 2010: Investigating soil moisture–climate interactions in a changing climate: A review. *Earth-Sci. Rev.*, **99**, 125–161, https://doi.org/10.1016/j.earscirev.2010.02.004.

Sheridan, S. C., and C. C. Lee, 2018: Temporal trends in absolute and relative extreme temperature events across North America. *J. Geophys. Res. Atmos.*, **123**, 112889–112898, https://doi.org/10.1029/2018JD029150.

Smith, R. J., 2009: Use and misuse of the reduced major axis for line-fitting. *Amer. J. Phys. Anthropol.*, **140**, 476–486, https://doi.org/10.1002/ajpa.21090.

Tamarin-Brodsky, T., K. Hodges, B. J. Hoskins, and T. G. Shepherd, 2019: A dynamical perspective on atmospheric temperature variability and its response to climate change. *J. Climate*, **32**, 1707–1724, https://doi.org/10.1175/JCLI-D-18-0462.1.

——, ——, ——, and ——, 2020: Changes in Northern Hemisphere temperature variability shaped by regional warming patterns. *Nat. Geosci.*, **13**, 414–421, https://doi.org/10.1038/s41561-020-0576-3.

Wang, Z., Y. Jiang, H. Wan, J. Yan, and X. Zhang, 2017: Detection and attribution of changes in extreme temperatures at regional scale. *J. Climate*, **30**, 7035–7047, https://doi.org/10.1175/JCLI-D-15-0835.1.

Wilks, D. S., 2011: *Statistical Methods in the Atmospheric Sciences*. Academic Press, 704 pp.

Zschenderlein, P., A. H. Fink, S. Pfahl, and H. Wernli, 2019: Processes determining heat waves across different European climates. *Quart. J. Roy. Meteor. Soc.*, **145**, 2973–2989, https://doi.org/10.1002/qj.3599.